Available online at www.sciencedirect.com
SCIENCE DIRECT®
Journal of volcanology and geothermal research
ELSEVIER
Journal of Volcanology and Geothermal Research 127 (2003) 121–152
www.elsevier.com/locate/jvolgeores

Controls on the growth and geometry of pyroclastic constructs

C. Riedel [1,*], G.G.J. Ernst [1,2], M. Riley

Centre for Environmental and Geophysical Flows, Department of Earth Sciences, University of Bristol, Wills Memorial Building, Queen's Road, Bristol BS8 1RJ, UK

Received 7 August 2002; received in revised form 23 April 2003; accepted 11 June 2003

Abstract

In regions of frequent low-energetic explosive eruptions such as cinder cone fields, ejecta cone forming eruptions are the prime hazard whether from roof collapse or as a hazard to aircraft safety. So, observations and data for ejecta constructs and construct-forming eruptions are systematically reviewed here to help gain insights into key processes involved. Numerical modelling and experiments are developed and complemented by novel analogue granular pile drainage experiments focusing on laboratory 'cinder cones'. Our review shows that the vertical elevation growth rate of cinder cones can be more than 100 m in the first week for intense cone-building eruptions. Ejecta construct grain size is most frequently centred around 10–40 mm, sometimes less. Plinian-style eruption columns, albeit with material substantially coarser than in full-blown plinian eruptions, are commonly observed during the cone-building phase. We show that these observations are not consistent with the classic, no-drag, ballistic model of cone growth and are more consistent with a new model where cones grow by accumulation of clasts falling from an eruption jet column. We also show that cone growth can be equivalently approached either as due to fallout from the margins of a jet or as accumulation obtained by tracking the paths of single particles in the drag case. Numerical experiments are carried out and compare well with morphometric data for ejecta constructs that preserve their primary depositional slope through welding. In the laboratory experiments, granular piles are built up to form a cone and then drained centrally to produce a crater. We explore how the granular pile nature of cones controls crater development and cone geometry. We report and rationalise a close match between experimental and natural cinder cones. Experiments also indicate that an increasing fraction of fine cohesive material accounts for inner crater slopes varying from 45° for cinder cones with little fine ash to near-vertical for ejecta cones rich in fine ash. This could be used in rapid hazard evaluation at little-known, cone-like, pyroclast-dominated volcanoes and in analyses of ejecta constructs on other planets.
© 2003 Elsevier B.V. All rights reserved.

Keywords: cinder cones; pyroclastic constructs; explosive eruptions; strombolian; laboratory experiments; cone-forming eruptions; volcanic hazards; volcano morphology; eruption model

[1] These authors contributed equally to this work.

[2] Present address: Research Centre for Eruption Dynamics, Department of Geology and Soil Science, University of Gent, Krijgslaan 281 S8, 9000 Gent, Belgium.

* Corresponding author. Present address: Institut für Geophysik, Universität Hamburg, Bundesstrasse 55, 20146 Hamburg, Germany.

E-mail addresses: riedel@dkrz.de (C. Riedel), gerald.j.ernst@bristol.ac.uk (G.G.J. Ernst).

0377-0273/03/$ – see front matter © 2003 Elsevier B.V. All rights reserved.
doi:10.1016/S0377-0273(03)00196-3

1. Introduction

1.1. Occurrence and significance of pyroclastic ejecta constructs

Pyroclastic ejecta constructs, the most frequent type of which are cinder cones or scoria cones, are the most common volcanic landform on Earth. They have also been documented on the Moon (McGetchin and Head, 1973; Vespermann and Schmincke, 2000; Spudis, 2000), Venus (e.g. Guest et al., 1992) and Mars (Wilson and Head, 1994; Fagents et al., 2002). Cinder cone fields make up 2% of all listed volcanic areas in the Catalogue of Volcanoes (Simkin and Siebert, 1994) and each of these fields can contain up to hundreds of cinder cones (Settle, 1979) and up to a thousand vents (Connor and Conway, 2000). Whereas many cinder and scoria cones are mined for important raw materials worldwide (Heiken, 2003), the main reason for studying cone-forming eruptions is the potential threat such eruptions pose to human populations and local activities. For example, Vesuvius has had a dozen cone-forming explosive eruptions since 1631 (Arrighi et al., 2001), and while Vesuvius is currently in its longest repose period since 1631, the recurrence of such eruptions is anticipated within some decades and will pose considerable hazards both on the ground (600 000 people living at Vesuvius' foot) and for air traffic (it will challenge the Toulouse Volcanic Ash Advisory Centre, which has not had to deal with severe volcanic crises yet).

Several large cities (e.g. Auckland, NZ; Portland, OR, USA; Mexico City; e.g. Cas and Wright, 1987) and a key astronomical observatory (Mauna Kea, Hawaii; Porter, 1972) are at least partly built on dormant cinder cone fields. A cinder cone north of Lake Tahoe has been used for sewage disposal, posing local pollution problems (Matthews and Franks, 1971). The storage of low- and medium-grade nuclear waste within a cinder cone field at Yucca Mountain, Nevada (Yucca Mountain Project/YMP, 2002) has been adopted by the US Government in July 2002, despite the reservations of many Earth scientists concerning the long-term geological stability and safety of the site (Connor et al., 2000). All these cinder cone fields were active less than 100 ka ago or much more recently, and few geologists would question that they may erupt again (e.g. Connor and Conway, 2000; Siebe, 2000), the latest example at the time of writing being the cone-growing episode on Nyamuragira volcano in August 2002 (Tedesco and Durieux, personal communication).

1.2. Specific illustrations of hazards from cone-forming eruptions

Injuries of individuals during these eruptions are common, e.g. in the case of the 1986 Pacaya (Guatemala) eruption, where single 25 cm sized bombs flew to distances of 3 km from the vent, crashed into houses in the town of Calderas (north of Pacaya) and injured 12 people (SEAN, 1986). In the case of cone growth near human settlements, the 1973 Eldfell eruption on Heimaey Island (Iceland) demonstrated vulnerability to such eruptions (Thorarinsson et al., 1973; Self et al., 1974). The whole island population had to be evacuated and more than one-third of the houses collapsed due to ejecta loading on roofs, an experience which was shared by the Mexican population during the eruptive episodes of Paricutín (Mexico) in the 1940s (Foshag and Gonzalez, 1956; Luhr and Simkin, 1993), and Xitle (Mexico) in archaeological times (Siebe, 2000).

A recent cinder cone-building episode at Etna (Italy) produced a thick grey ash plume (tracked for hundreds of kilometres on satellite imagery) on 19th July, 2001, before the cone started to grow visibly on the 25th July (Behncke, 2001; Behncke and Neri, 2002). Ash fallout led to closure of Catania airport on several days. Similarly, during the October 1983 Miyake-jima eruption (Japan), the local airport had to be closed for 4–5 days (McClelland et al., 1989, pp. 283–287). As the above are but a few examples taken from among many, there is concern that even mildly to moderately explosive cinder cone eruptions can create significant hazards for the human population and for the economy on the ground, including airport operations, and for air traffic.

1.3. Review of some key features of ejecta constructs

Exactly how ejecta constructs erupt and grow is thus crucial for hazard assessment and industrial exploitation of volcanic ejecta. Here we use the term *pyroclastic ejecta constructs* to include *spatter cones*, *littoral cones* (or *pseudocones* associated with rootless craters), *tuff 'cones'* (e.g. Cas and Wright, 1987) and *ultraproximal cones* (those forming the near-vent continuation of plinian-sheet fall deposits; Ernst, 1996; Fierstein et al., 1997).

Most of these are typically thought to be characterised by *monogenetic* eruptions, i.e. through a single vent, or one or a few focal points along a fissure (e.g. Cas and Wright, 1987). However, phases of cinder/scoria cone-building activity also occur at stratovolcano and caldera complexes (e.g. DiVito et al., 1987; McClelland et al., 1989) and even in submarine environments (McInnes et al., 2001), although these have not been studied systematically.

The material of cinder cones consists of welded and/or unwelded scoria lapilli and loose coarse ash (e.g. Macdonald, 1972). Typically, numerous blocks and bombs amount to a characteristic but volumetrically minor fraction of the construct. A key point is that the median particle size of the material normally is in the range 1–4 cm (see Table 1) instead of 10 cm or more as reported in the classic cinder cone growth modelling of McGetchin et al. (1974).

A further key feature, often overlooked, is that 50% of the ejected volume or more may be deposited as a widespread ash blanket beyond the cone itself. Two striking examples of this are Cinder Cone (Lassen Peak National Park, CA, USA; Heiken, 1978) and Paricutín (see Wood, 1980 and references therein, for a review). Examples where ash blankets extend tens of kilometres beyond the cinder cone include Cerro Negro (Nicaragua; McKnight and Williams, 1997; Hill et al., 1998; Connor et al., 2001), Fuego (Guatemala; Bonis and Salazar, 1973; Rose et al., 1978) and Xitle volcano (Mexico City; Siebe, 2000).

1.4. Previous modelling work on ejecta construct growth and its limitations

Most of the modelling work on ejecta construct growth has focused on cinder cones and on the role of *ballistic ejection* (e.g. Chouet et al., 1974; McGetchin et al., 1974; Dehn, 1987; Bemis, 1995; Bemis and Bonar, 1997). This is often termed *Strombolian activity* (Jaupart and Vergniolle, 1997; Vergniolle and Mangan, 2000).

A key assumption of these models is a typical particle size of 10 cm in diameter (McGetchin et al., 1974). Indeed, particles smaller than this size are normally thought of as unable to follow ballistic trajectories (Sparks et al., 1997). From the above and from median-size data in Table 1, it is clear that the (no-drag) ballistic model only applies to late-stage weak-intensity events and/or to rare coarse-grained cinder cone eruptions (e.g. Etna NE Crater 1973; McGetchin et al., 1974) as most cinder cones are much more fine-grained (see Table 1). We agree that grain-size data for cinder cones may be affected by impact breakage to some extent (McGetchin et al., 1974; Self et al., 1974), but the effect of breakage on grain-size distribution has not been *quantified* to unambiguously show this.

The ballistic ejection model can hardly account for the formation of an ash blanket extending beyond the cone. To account for such cone-associated ash blankets, two new dispersal models have recently been developed (Parfitt and Wilson, 1999; Connor et al., 2001), based on the concept that cone-forming eruptions can generate ash-clouds as well as widespread ash fall deposits as in plinian-style eruptions. The Parfitt and Wilson (1999) and Connor et al. (2001) models, however, do not focus on aspects related to cone growth, which are the central themes of the present paper.

There is also photographic documentation and field data for some classic cinder/scoria cone eruptions (e.g. Paricutín 1943; Heimaey 1973; Pagan 1981; Miyake-jima 1983; Oshima 1986; Lonquimay 1989; Fogo 1995; Etna 2001; see Table 1), unambiguously demonstrating that at least in the initial phase of activity, which may last for days to weeks, a plinian-style ash-rich column extend-

Table 1
Properties of ejecta cones and their cone-building eruptions

Cone	Area	Eruption date	Median grain size	Average sorting	Cone height/time	Cone diameter (m)	Max. plume height (km)	Eruption velocity (m s^{-1})	Max. ballistic ejection height (m)
Anak Krakatau [1]	Indonesia	1979	fine ash		150 m/2 d		2	150–170	500
Ardoukoba1 [1]	Djibouti	1978					0.3		70
Beerenberg [1]	Jan Mayen	1984	ash				1		
Cerro Negro [2]	Nicaragua	1995	0.7 mm				1–2	100–120 [3]	400 [4]
Cinder Cone/Lassen Peak [5]	California	n.h.	0.8–3 mm [5]	1.4			unknown	unknown	unknown
Cone I/Tolbachik [6]	Kamchatka	1975	> 2 mm [7]		85 m/18 h	438	6–8	200	400
					125 m/67 h	600			
					135 m/81 h	700			
					145 m/91 h	750			
					165 m/118 h	900			
Eldfell/Heimaey [8]	Iceland	1973	6 mm	1.1	120 m/68 h[9]		5–7.3 [9]	150 [10]	400 [9]
					160 m/130 h				
					180 m/168 h				
Cone del Lago/Etna [11]	Italy	2001			50 m/2 d, 100 m/4 d	250	0.2 [12]		300 [12]
NE crater/Etna[13]	Italy	1969/70	1 cm (bulk)	~4	40–50 m	200	yes (unknown altitude) [12]	51	400
			10 cm (ballistic)	~1.5					
Fogo [14]	Cape Verde	1994	?		120 m/84 h		2–5	unknown	600
Galiarte[34]	Azores	n.h.	0–0.5 km/25 cm+	small					
			0.5–1 km/< 25 cm						
			1–1.3 km/< 10 cm						
			1.3–2 km/< 5 cm						
			2–3 km/< 2.5 cm						
			> 3 km/< 1 cm						
Galunggung [15]	Java	1982	ash		70–80 m	200	16		
Hekla [16]	Iceland	1970			100 m		15		
Kaalkoppie [17]	Marion Isl.	1980	lapilli and ash		6 m				
Kapoho/Kilauea [18]	Hawaii	1966	?		30 m/3 d		no plume		
					50 m/4 d				
Kliuchevskoi [1]	Kamchatka	1980			20 m/1 d		5		
Lathrop Wells [19]	Nevada	n.h.	1 cm	1.2			unknown	unknown	unknown
Long Island [20]	Papua New Guinea	1973	ash and cinder						10
Miharayama/Izu-Oshima [21]	Japan	1986	2–8.2 cm [33]		40 m		16		500
Miyake-jima [1]	Japan	1983	ash				10		
Monte Nuovo/Campi Flegrei [22]	Italy	1538	4–64 mm	~1–2	65 m/1 d		4–5	unknown	unknown
Murara/Nyamuragira [1]	Zaire	1976/77	lapilli		150 m/25 d				500–600
Navidad Cone Lonquimay [23]	Chile	1988	0.3–3 mm [24]		50 m/1 d	80	5.5–6	300	unknown
					60 m/3 d	150			
					100 m/4 d	250			
					110 m/5 d	250			
					180 m /6 d	250			
					> 200 m/10 d	300			

Table 1 (*Continued*).

Cone	Area	Eruption date	Median grain size	Average sorting	Cone height/time	Cone diameter (m)	Max. plume height (km)	Eruption velocity (m s^{-1})	Max. ballistic ejection height (m)
North Pagan [25]	Mariana Islands	1981	ash and lapilli		80 m/13 d		13		
Pacaya [26]	Guatemala	1987	6–10 cm						
Pacaya[1]	Guatemala	1981			15 m/6 d		0.3		100
Paricutin[27]	Mexico	1943	?		6 m/2 h 8 m/6 h 11 m/10 h 25 m/12 h 30 m/15 h 44 m/2 d 106 m/7 d 148 m/28 d	 70 ~400	>2.5	200	500
Rothenberg/Eifel [28]	Germany	n.h.	4 mm 64 mm	2 0.5			unknown	unknown	unknown
Serra Gorda [32]	Azores	n.h.	0–3 km/4cm+ 3–6 km/<4 cm >6 km/<2 cm	~1	~200 m			unknown	unknown
Sierra Negra [1]	Galapagos	1979	5–10 mm						
Songeong Api [1]	Indonesia	1985	ash				12		
Stromboli[29]	Italy	1973	22–25 mm [29]				no plume	2.5–75 [29]	
Teneguia I/La Palma [30]	Canary Islands	1971	lapilli and bombs		150 m/120 h 180 m/168 h		no plume	unknown	400
Tinakula [31]	Solomon Islands	1971	cinder		15 m		0.3		
Ulawun [20]	Papua New Guinea	1973	ash and bombs				2		
Veniaminoff [1]	Alaska	1983	ash		150 m/7d	500	6		250

A lot of these eruptions are coincident with a plume. Their growth is given as cone height after hours (h) or days (d). Where known, the diameter has been given to test Wood's equation. The maximum ballistic ejection height can be used as an estimate of ejection velocity. n.h. = non-Holocene. References are from: [1] McClelland et al., 1989; [2] Hill et al., 1998; [3] Global Volcanism Network, 1995b; [4] Global Volcanism Network, 1995a; [5] Heiken, 1978; [6] Tokarev, 1983; [7] Budnikov et al., 1983; [8] Self et al., 1974; [9] Global Volcanism Network, 1973; [10] Blackburn et al., 1976; [11] Pfeiffer, 2001; [12] Behncke, 2001, [13] SEAN, 1988; [14] Global Volcanism Network, 1995c; [15] Suradjat and Siswowidjo, 1984; [16] Thorarinsson et al., 1973; [17] Verwoerd et al., 1981; [18] Richter et al., 1970; [19] Wohletz, 1986; [20] Cooke, 1975; [21] Earthquake Research Institute (ERI), 1988; [22] DiVito et al., 1987; [23] SEAN, 1988; [24] Global Volcanism Network, 1989; [25] Banks et al., 1983; [26] SEAN, 1986; [27] Foshag and Gonzalez, 1956; [28] Houghton and Schmincke, 1989; [29] Chouet et al., 1974; [30] SEAN, 1974; [31] Thompson, 1973, [32] Self, 1976, [33] Sumner, 1998.

ing vertically up to 20 km above the vent is commonly generated (Table 1). When observations are made at night, it becomes clear, however, that much of the mass is distributed in a lava fountain (Parfitt, 1998; Sumner, 1998; Parfitt and Wilson, 1999) as well as within the jet (i.e. momentum-dominated), lowermost region of the eruption column. This is in contrast to full-blown plinian columns, where ca. 90% of the particles are finer than 1 mm (Sparks et al., 1997) and are thus carried to the very top of the column and into an umbrella cloud, due to the vigorous re-entrainment of the falling particles (see Ernst et al., 1996).

There is also a considerable amount of confusion in the use of terms in reports of ejecta-construct building activity and descriptions of deposits produced. Most of the terms (see below) are routinely used interchangeably without much thought given to defining what is meant. This results in insufficiently clear descriptions. Such descriptions are potentially invaluable to advance our understanding of how eruptions work but cannot be used because of their ambiguous nature. The above review of ejecta construct activity and deposits demonstrates that vigorous cinder cone-forming eruptions are not dominantly *strombolian* in dynamic character (i.e. *strombolian-style*) but simultaneously *hawaiian* (lava fountain) and *subplinian* (eruption column; see also discussion about the 1783 Asama eruption by Yasui et al., 1997; Yasui and Koyaguchi, 1998). By *strombolian-style*, we mean weak-intensity, strongly intermittent activity observed to be associated with bursting of large gas bubbles extending across much of the vent, and producing ballistic emplacement of clasts $\gg 10$ cm (Blackburn et al., 1976). Realising the ambiguity in the use of the term '*strombolian*', in some instances the term *violent strombolian* has been used instead to account for eruptions which, being accompanied by a sustained eruption column, are thus *subplinian* in dynamical character (i.e. *subplinian-style*) but for which the deposit dispersal is too moderate to speak of subplinian eruptions (see Walker, 1973; see also Arrighi et al., 2001). Part of the confusion arose because the eruptions were classified based on their deposits, which means that an eruption can be classified as *strombolian* even when it has been observed to have been *hawaiian* (Parfitt and Wilson, 1999; E. Parfitt, personal communication) or *subplinian* (this paper) in character. The *hawaiian-style* Kilauea Iki and Pu'u'O'o eruptions, for example, produced deposits with a dispersal area suggesting *strombolian* events. If the cones had not been directly observed to have resulted from deposition by lava fountains, their formation may have been incorrectly attributed to intermittent *strombolian* explosions (E. Parfitt, personal communication). In the low explosivity range, dynamic style is thus not necessarily indicated by deposition, i.e. cinder cone-forming events are not necessarily tied to *strombolian*-style eruptions, as defined above. They can be associated with *ashclouds* tracked by satellites to be at least up to 400 km long and 200 km wide (e.g. Etna in July 2001; Behncke and Neri, 2002), and with *small-volume pyroclastic flows* (PF) (e.g. a 4 km long PF at the Sangeang Api 30 July 1985 eruption; McClelland et al., 1989, pp. 217–218; or PFs of 0.5 km length during the 24 Sept. 1986 NE Crater eruption of Etna, during the strombolian termed activity of Ulawun in 1975-Cooke, 1975, and during Cerro Negro eruptions).

In classic examples (e.g. Paricutín, Lonquimay, Tolbachik), a key visual observation by ground observers is that cones grow at a rapid rate in the first few days of activity by *fallout* from the margin of an eruption column followed by coeval mass redistribution by grain flow avalanching on the growing cone (e.g. Luhr and Simkin, 1993 and references therein). Several cones have been documented to have grown by around *160 m* in elevation *in* less than *6 days* of activity (Table 1). Most of the material ejected is *fine-grained* and hardly any of it could be thought of as ballistic-size material. In our view, impact breakage cannot account for a significant part of the grain-size distribution in most cases. We want to quantify the contribution of impact breakage to airfall grain-size distributions in future work.

Spatter mounds and ramparts and some ejecta cones are also observed to be produced wholly or partly by hawaiian lava fountains (and/or the lower region of eruption columns which may include a lava fountain). Latest modelling of lava foun-

taining eruptions concluded that these eruptions can be considered, in dynamical terms, as plinian eruptions for which most of the material is coarse-grained and only a small fraction of the erupted mass partitions into the gas-rich buoyant plume forming above a *lava fountain* (Parfitt and Wilson, 1995, 1999; Yasui et al., 1997; Yasui and Koyaguchi, 1998), itself reaching *up to 2 km* above the vent (e.g. Sumner, 1998).

Construction of a thick pile of ejecta around the vent is not limited to hawaiian, strombolian and subplinian-style events but also extends to full-blown *plinian* eruptions. In plinian eruptions where ultraproximal deposits are preserved (e.g. Tarawera 1886, Quizapú 1932, Novarupta 1912; Ernst, 1996; Fierstein et al., 1997), the plinian sheet of fallout is seen to evolve laterally into a *cone of ejecta* surrounding the vent. The 1912 Novarupta (Alaska) ultra-proximal cone, for example, has a maximum height reaching up to 250 m and a diameter of ca. 1 km (Fierstein et al., 1997). Cone-forming deposits such as this have been interpreted to be the result of ballistic ejection which took place from the side of the vent while plinian activity was ongoing through the same vent (Fierstein et al., 1997). We find it difficult to reconcile this with the fact that the ejecta are much finer-grained, on average, than what is expected from intermittent ballistic ejection and deposition (Ernst, 1996). A much simpler explanation, consistent with the detailed field data collected by Fierstein et al. (1997), for the origin of such cones is fallout and/or ejection from the margins of the lowermost region of the plinian column. This region of a plinian column is momentum-driven and characterised by extreme marginal shear resulting in the impulsive growth of large eddies at the eruption jet margin. The centreline velocity also decreases much more rapidly in this initial jet region (as $1/Z$, over a short height range of a few kilometres at most) than elsewhere in the column (where the centreline velocity may actually accelerate and then decrease at a much more gradual rate, scaling approximately as $1/Z^{1/3}$; see Ernst et al., 1996; Sparks et al., 1997).

In sum, we argue that alternative models for the growth of cinder cones or scoria cones, ultra-proximal ejecta cones associated with plinian eruptions, and spatter cones from intense lava fountains are needed which can account for the subplinian character, for the role of the eruption jet column, for the associated column fallout (and avalanching), and the rapid initial growth.

1.5. Observations and data on cinder cone geometry and aspect ratio; types and geometry of pyroclastic constructs

Here we account quantitatively for the ejecta constructs described above by reviewing the types and geometry of constructs to enable comparisons between new experiments and modelling predictions in later sections of the paper.

Wood (1980), who considerably extended the classic study of Porter (1972), is the primary source for the geometry of cones. These authors found the outer slope of recently erupted cones to be overwhelmingly at the angle of repose for loose granular material, although depending slightly on grain size. This repose angle is ca. 30–33°. Older cones are often compacted, subsided or eroded. These secondary processes reduce the outer slope angle and can increase the crater rim diameter (e.g. Sohn and Park, 2003). The record of this evolution was used effectively to semi-quantitatively date older cinder cones (Wood, 1980). The inner crater slope of young cones, in particular, was found to be about 10–15° steeper than the outer slope, but this key observation was never accounted for.

1.5.1. Cinder cones

Characteristic cinder cone morphology and tectonic emplacement have been described previously (Porter, 1972; Settle, 1979; Wood, 1980; Hasenaka and Carmichael, 1985; Carn, 2000; Ferreira, 2000). Whereas non-eroded cinder cones externally show a linear or slightly convex shape, eroded cones tend to display concave slopes (Dohrenwend et al., 1986). Characteristic (i.e. mean values) geometrical aspect ratios defined using crater width (W_{cr}), base diameter (W_{co}) and crater-rim to cone-base height (H_{co}) (see Fig. 1) are mostly constant on recently erupted, non-eroded cones (Porter, 1972; Wood, 1980):

$$\frac{W_{cr}}{W_{co}} \approx 0.4 \text{ and } \frac{H_{co}}{W_{co}} \approx 0.18 \quad (1)$$

Similar *Porter and Wood (PW) ratios* have been confirmed, for fresh cones, by recent studies at Lamonggan (Indonesia; Carn, 2000), the Michoacán-Guajuanato field (Mexico; Hasenaka and Carmichael, 1985) and Sao Miguel Island (Azores; Ferreira, 2000). Statistically, the PW ratios appear to be mean values with reasonably narrow standard deviations based on measurements of a relatively large number of cones, albeit from a comparatively small number of cone fields (the bulk of the data is from Mauna Kea in Hawaii, from the San Francisco Volcanic Field of Arizona, and from the Lamonggan volcanic field of Indonesia). The morphological ratios have been used to provide insights into the history of extraterrestrial volcanoes (Wood, 1977) or for hazard prediction, e.g. in the case of Cerro Negro (Nicaragua), in order to decide whether large-scale plinian eruptions and the associated hazards are to be expected (McKnight and Williams, 1997).

Cinder cone fields occur in both relatively flat areas and on the flanks of composite or shield volcanoes and are consequently divided into *platform* and *volcano cone fields* (Settle, 1979). The PW ratios (once again, we stress that they are mean values) above, however, are constant irrespective of setting (Wood, 1980), although we feel that this should be further scrutinised in future by collecting datasets (including age and meteorological constraints) from tropical and subtropical settings for which fewer data are available. Bemis (1995), for example, studied numerous cones from Guatemala and measured the morphological ratios there, suggesting that even the mean of these ratios may not always be constant. However, at this point, little else can be added about this without additional data as the ages of the well-preserved cones examined by Bemis are currently unknown.

Eqs. 1 are valid for cones that have reached the angle of repose, i.e. for which small additions of mass can produce avalanching at any point. That it is so has been observed in the field by McGetchin et al. (1974). We are not aware of any fresh cinder cone, which, after eruption, would not have been found at the angle of repose. During eruptions, we are not aware of any cinder cone which would not have reached the angle of repose early on in the cone-building eruption.

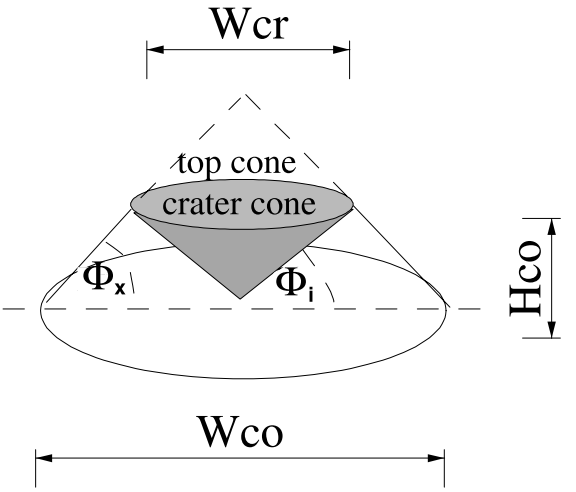

Fig. 1. Generic sketch illustrating the basic geometry of ejecta constructs made up of loose granular material. The basic geometry is often (near-)conical as illustrated here. Most characteristic ejecta cones exhibit a crater reaching down to their baseline. Crater diameter W_{cr}, cone diameter W_{co} and cone height H_{co} can be used to calculate the cone volume by subtracting the volume of the top cone and the crater (inverse) cone from the big cone.

Using Eqs. 1, a key deduction (not previously made in the correct form), which is important e.g. for comparing magnitudes of diverse cone-building eruptions, is that the volume of a cinder cone is entirely defined if cone height H_{co}, is known (Fig. 1). For ejecta cones for which the crater is centred below the summit of the large completed cone that is obtained by prolonging the outer surface upward, cone height H_{co} and cone volume V are related as:

$$V = \pi H_{co}^3 \left(\frac{1}{\tan^2 \Phi_x} + \frac{2}{\tan^2 \Phi_i} + \frac{3}{\tan \Phi_x \tan \Phi_i} \right) =$$

$$\pi H_{co}^3 \left(\left(\frac{W_{co} - W_{cr}}{2H_{co}} \right) + \frac{W_{cr}^2}{2H_{co}^2} + \frac{3W_{cr}(W_{co} - W_{cr})}{4H_{co}^2} \right)$$

$$\approx 11.5 H_{co}^3 \quad (2)$$

where Φ_x is the cone's outer slope angle and Φ_i is the internal crater slope angle (Fig. 1). Eq. 2, as illustrated in Fig. 1, can be readily deduced by

subtracting the volumes of the inverse crater cone and the top cone from the volume of the whole cone formed by the base diameter and a pointed top with a slope Φ_x.

The same result can also be obtained by integrating the volume of the deposit ring over rotation angle. In the case of non-negligible vent radii compared to cone base diameter (e.g. tuff cones), the integration method provides a more accurate estimate of the deposit volume more easily.

Hasenaka and Carmichael (1985) presented a formula which did not subtract the crater inverse cone in their calculations of cinder cone volume, i.e. they implicitly assumed that the crater of a cinder cone is *always* filled with material. This is a valid assumption mostly for old cinder cones where the crater becomes filled through secondary processes (see e.g. Rothenberg; Houghton and Schmincke, 1989). However, in the case of Paricutín for example, where the crater geometry was documented over several years of activity, a close correlation between W_{cr} and the height of ash columns at the corresponding time suggests that the crater is enlarged both by landsliding and slumping in the vent during quiet periods, and by erosion or remobilisation of material on the inner crater surface due to explosive activity in the crater (Wood, 1980). Here, we also carried out analogue laboratory experiments (see new experiments hereafter) which suggest that during eruptions most cinder cones have an inverted cone-shaped crater extending down to the cone baseline. In our experiments, the crater only forms by downward drainage of a granular pile and not by forceful erosion from explosive activity. However, the fact that W_{cr}/W_{co} at Paricutín remained near-constant over several years, irrespective of whether crater enlargement occurred by drainage during quiet periods or erosion during explosive phases, suggests that controls on crater and cone geometry and static stability are identical irrespective of crater formation mechanism.

In sum, to determine deposit volumes during cone-formation the crater volume should be subtracted from the volume of the truncated cone (i.e. with trapezoidal vertical cross-section) assumed by Hasenaka and Carmichael (1985), in order to improve on their estimations of cone volumes.

1.5.2. Pseudocones

Pseudocones (with *pseudocraters*) are small copies of their large counterparts, cinder cones. The pseudocones described in the classic study for Lake Myvatn, Iceland (Rittmann, 1938) are all built from lapilli-sized basaltic tephra particles. A majority exhibits the typical ratios of cinder cones ($W_{cr}/W_{co} \approx 0.4$), e.g. Kleifarholar and Geitey. Pseudocone deposits do not differ much geometrically from cinder cone deposits, so in the present paper, their growth, sedimentation and avalanching dynamics is proposed to be identical to processes in cinder cones.

1.5.3. Spatter 'cones'

The growth of spatter cones, ramparts or hornitos can in some cases be closely related to the growth of cinder cones (e.g. Macdonald, 1972). Typical examples include the Kapoho phase of Kilauea (Richter et al., 1970), the eruptions of Piton de la Fournaise, La Réunion (Montaggioni et al., 1972; Krafft and Gerente, 1977) or the eruption of Miharayama, Japan 1986–1987 (ERI, 1988). Rittmann (1938) already reported the remnants of spatter cones inside the eroded structures of pseudocones. These accounts of spatter cone eruptions suggest that the initial growth of a spatter cone is often overprinted by the subsequent growth of what appears to be a cinder cone. At Pu'u'O'o (Neal et al., 1987; Wolfe et al., 1988), Kilauea Iki (e.g. Parfitt and Wilson, 1999) and on Lanzarote (Carracedo et al., 1992), however, Parfitt argues that although the main vent constructs appear as cinder cones, they are in fact hawaiian spatter cones (Parfitt, personal communication; see below). When examined in detail by Parfitt (1998; personal communication, 2002) they appeared to be dominated on the surface by large, deformed and strongly welded clasts. Parfitt concludes that they are not cinder cones at all. One should also consider, however, that later-stage activity from a cinder cone-building eruption may (again) produce spatter for a short period (as gas content and eruption rate decrease or temperature increases in the conduit).

The surface deposition of spatter, in effect, could readily cover up the dominant cinder cone nature of at least some constructs. Clearly, this brief discussion indicates that more detailed and systematic field work on cinder and spatter cones is needed.

With the exception of the early cones or ramparts these cones were reported not to exhibit typical spatter cone slopes (which we document quantitatively hereafter for the first time), but typical constant-gradient cinder cone slopes. Whereas these *spatter-cinder cones* can eventually grow to heights typical of cinder cones, pure *spatter cones* appear to grow only up to heights of 20–30 m (cf. examples on Mt Etna; Green and Short, 1971; or Piton de la Fournaise; Lénat et al., 2001), and generally less than 10 m (Cas and Wright, 1987).

The outer slopes of pure spatter cones can be near-vertical close to the vent. When they grow larger than a few metres, they exhibit slopes controlled by rapidly decreasing construct height with increasing distance from vent. These slopes are investigated here by digitising the slopes presented on photographs from the initial Pu'u'O'o 'cone' (USGS slide set on *Volcanoes in eruption*) and three Etna spatter 'cones' (Green and Short, 1971) (Fig. 2), i.e. four examples of the largest spatter constructs. A best fit by simple functions is presented in section 2 (illustrating that pure spatter 'cones' are clearly not conical in geometry, unlike cinder cones). The importance of spatter cone slopes for our numerical modelling will become clear in section 2.

1.5.4. Ultraproximal cones

Ultraproximal (plinian) cones build up around the vent during plinian (Ernst, 1996) or subplinian eruptions (e.g. 1783 Asama; Yasui and Koyaguchi, 1998). We argue that these coeval near-vent constructs of plinian events also form by fallout from the momentum-driven or jet region of the eruption column. Typical examples of ultraproximal cones include the deposits of 1886 Tarawera (New Zealand; Walker et al., 1984), 1912 Novarupta (Alaska; Fierstein et al., 1997) and 1932 Quizapú (Chile; Hildreth and Drake, 1992) eruptions.

Their internal crater slopes are usually very steep and do not resemble a typical redistribution by avalanching, but rather collapse structures as documented for collapse calderas (e.g. Martí et al., 1994; Roche et al., 2000; Walter and Troll, 2001). The crater width is usually much wider than that typical for recently erupted cinder cones. There is only a small fraction of the cone ejecta which is in the ballistic range in terms of grain size. Therefore there must be an alternative model to the strombolian-style ballistic ejection model (see Fierstein et al., 1997) accounting for the formation of such cones.

We emphasise that if deposition from the lowermost region of eruption columns is responsible for the formation of such cones, they should *always* form during plinian eruptions. They may not have been described previously, apart from the examples already mentioned and for which preservation is unusually continuous and complete, because most fall deposits will typically be buried by pyroclastic density currents, thick intracaldera fill or inaccessible in a lake or the sea flooding the crater, or dismissed as a proximal accumulation of ballistically emplaced ejecta (Ernst, 1996).

1.5.5. Tuff cones

Tuff cones have been described in detail by Sheridan and Wohletz (1983), Wohletz and Sheridan (1983), Wohletz (1986), Houghton and Schmincke (1989), Sohn (1996), Vespermann and Schmincke (2000) and Sohn and Park (2003). They are believed to grow in monogenetic hydrovolcanic eruptions such as those observed on Surtsey (Iceland) in 1963 (Thorarinsson, 1964). Their internal crater slopes of up to 45° result in ratios of $H_{co}/W_{cr} \approx 0.2–0.5$ (Vespermann and Schmincke, 2000), which scatter around the characteristic cinder cone value. The phreatomagmatic nature of fragmentation and deposition of base surges contributing to tuff cone growth lead to a grain-size distribution skewed towards the fines (Sheridan, 1971).

Considering initial phreatomagmatic phases at apparent cinder cones such as Eldfell (Global Volcanism Network, 1973), Tolbachik (Budnikov et al., 1983) or Monte Nuovo (DiVito et al., 1987), the difference between tuff cones and cinder cones

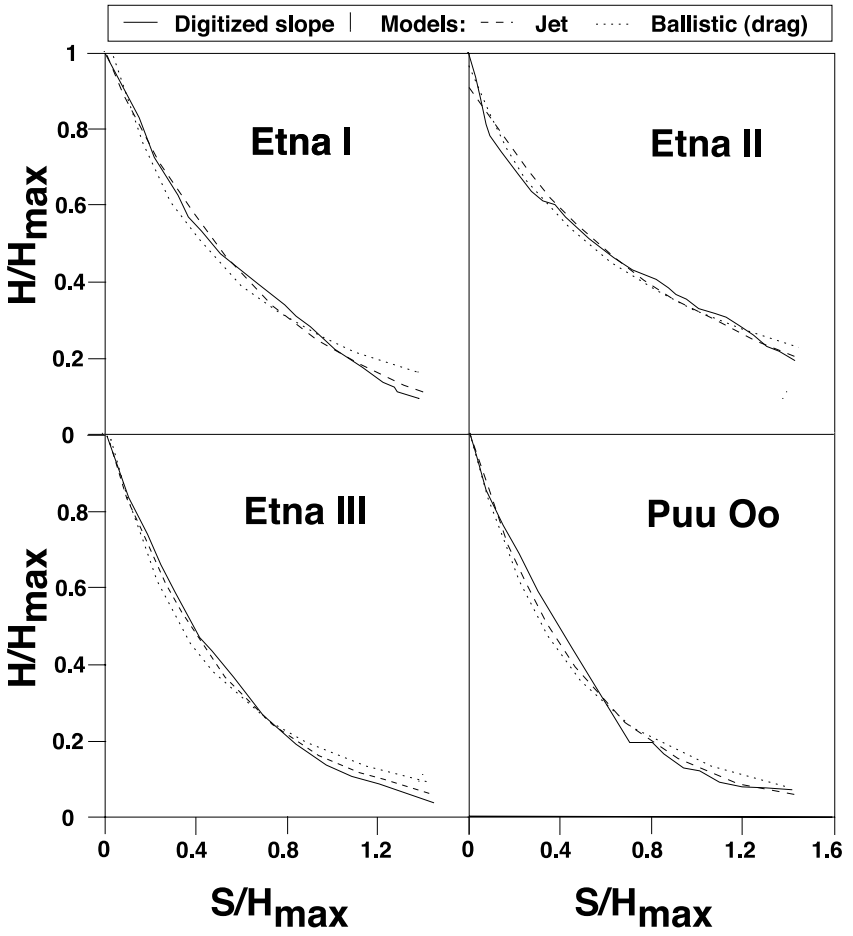

Fig. 2. Geometrical data for ejecta mounds for which clast fusing preserves the primary deposition slope. Four spatter cone slopes have been digitised from photos available on the web (Behncke, 2001; Etna III), Green and Short, (1971; plate 125A; Etna I/II) and the *USGS slide set* (Pu'u'O'o). To quantify the slopes of these constructs, simple functions have been approximated to the digitised slope trends. The dotted curve represents a $f(x) = A/xe^{Bx}$ type of curve, corresponding to predicted ballistic deposition trends (see text), whereas the dashed line is a curve of type $f(x) = (A/x - B/x^2)e^{Cx}x^D$, corresponding to the prediction for fallout from the margins of an eruptive jet. This jet fallout curve appears to most closely account for digitised data for spatter mound slopes (see also discussions in text).

partly blurs. Drilling near Eldfell and Surtsey has revealed that the basal sequence of phreatomagmatic-initiated cinder cones and surtseyan tuff cones is nearly identical (Tomasson, 1967): explosion-breccia overlain by base surge deposits (Houghton and Schmincke, 1989; Houghton et al., 1999). We realise that there are other typical tuff cone examples, e.g. Diamond Head, Hawaii (outer slope 20°/inner crater slope 25–30°) or Cerro Colorado, Mexico, where the inner crater slopes are near-vertical (Wohletz and Sheridan, 1983) and which differ substantially from those of cinder cones. However, a large number of tuff cones seem to form by similar deposition processes as cinder cones, even if their craters are much larger. Sohn (1996) already proposed that tuff cone building eruptions are dominated by inertia-driven jet activity.

Following the review we account for the observations by a numerical and a laboratory study for the deposition in and outside the crater. First we compare the classic strombolian no-drag model of ballistic ejection (McGetchin et al., 1974) with a numerical model of construct growth by fallout

from a turbulent jet. In a similar treatment to that adapted by Parfitt (1998) and by Parfitt and Wilson (1999), a jet is regarded here as a reasonable approximation for the lava fountain and lowermost region of a fairly coarse-grained eruption column, from which most of the clasts are too coarse to partition into the plume region. For loose granular ejecta constructs, we show how the shape of the cones is controlled by avalanching processes. A series of laboratory experiments documents a most remarkable similarity between the shape of pyroclastic cones and granular piles, and we briefly discuss its physical meaning. Wider implications for volcanic hazards and future work needed are also briefly considered.

2. Numerical modelling of cone growth

2.1. General

In this section, we develop numerical models which predict how the supply to growing ejecta constructs is expected to be distributed, prior to redistribution by surface avalanching, following physical models of *either* ballistic ejection or jet fallout sedimentation, *or* a combination which is explored by incorporating the effect of gas drag on clast transport. Ballistic ejection is initially developed according to the classic model of a strombolian event of McGetchin et al. (1974).

Hereafter we demonstrate that at least some cinder cone eruptions (probably the initial phase of most) can be accounted for by the fallout from the margins of a sustained jet, which typically transfers the mass from the conduit to an eruption column as in plinian-style events. In the past transient jets have been associated with 'strombolian' eruptions which are strongly intermittent (Chouet et al., 1974; Vergniolle et al., 1996; Vergniolle and Mangan, 2000), but sedimentation from either transient or steady jets to account for ejecta constructs has not been studied.

In all jet fall models (except for the ballistic models with drag), we assume that all particles are accelerated by the same initial process stemming from the conduit and possess the same similar initial velocity v_{erup} as the fluid erupted from the conduit independently of particle size, which, following Chouet et al. (1974), corresponds to a small particle (or dynamic equilibrium) approximation (valid for particles $\ll 10$ cm). Investigations of Knudsen and Katz (1958) suggested that the velocity profile across a rigid-walled conduit system is nearly flat at the huge Reynolds numbers involved in explosive volcanic eruptions. This motivated our simplifying assumption of a constant velocity across the conduit.

Typical particle (fluid) velocities are thought to be in the range from 10 to 200 ms^{-1}, spanning the range suggested in Table 1, depending on water content (Cas and Wright, 1987).

In order to account for the volume of the accumulating deposits, fallout models are dependent on particle volumes and thus on their grain size. Grain-size distributions in deposit descriptions are given either by a log-normal distribution (i.e. by median grain size and Inman sorting) or by particle weighting data. Both kinds of data were used here as input for modelling (see Table 1 and Fig. 3).

2.2. Ballistic ejection model (McGetchin et al., 1974)

McGetchin et al. (1974), Chouet et al. (1974) and Head and Wilson (1989) presented a model of particles ejected by lava fountains at an angle up to 30° from the vertical and travelling along ballistic trajectories. Clasts are emplaced where they land, and accumulate over time. The integrated volume of all these particles makes up the cone volume. Following deposition, the particles on the slopes undergo avalanching once the pile has built up beyond the angle of repose and this process determines the ultimate shape of the cone.

In more recent calculations, deposition modelling has been developed further by accounting for drag forces on the particles during flight (Dehn, 1987; Bemis and Bonar, 1997). Here we also compare a model without drag forces to one with drag forces. Both ballistic models are computed mainly for comparisons with data and with the new jet fallout predictions developed in section 2.3, and

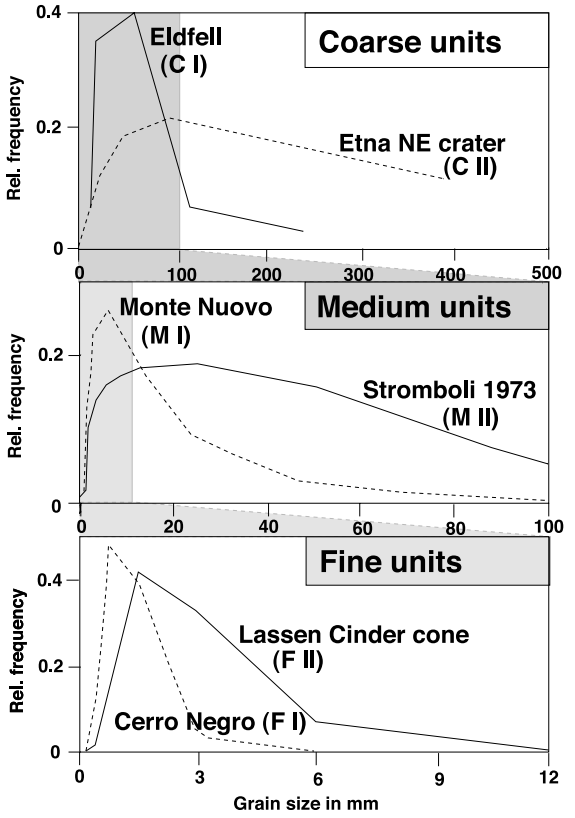

Fig. 3. Grain-size distributions (GSD) of typical ejecta constructs. The curves are either following published grain-size distributions [Heimaey (Self et al., 1974), Monte Nuovo (DiVito et al., 1987) and Stromboli (photoballistics; Chouet et al., 1974)] or log-normal distributions if only median grain size and Inman sorting are published [Etna NE crater (McGetchin et al., 1974); Cerro Negro (Hill et al., 1998) and Lassen Cinder Cone (Heiken, 1978)]. The curves comprise all the grain-size distributions given in Table 1, but only the extreme values of three different scale orders of grain sizes are illustrated (note *x*-axis scale varies). These grain-size distributions are used as generic distributions in the numerical experiments discussed in the paper.

to provide insights. As it turns out, we will show that this comparison is helpful, as it appears that one can successfully model cone growth by using a (ballistic) trajectory model accounting for drag (especially for particles of 'intermediate' sizes, in the 1–10 cm range) or by using a model focusing on fallout from the margins of an eruption jet. The two approaches appear to be two equivalent descriptions of the same process.

Let us consider first the problem of ballistic emplacement without drag. Assuming radial symmetry the problem can be formulated in two dimensions. The ballistic trajectories without drag forces are simply described in r and z coordinates by:

$$r = v_r t \tag{3A}$$

and

$$z = v_z t - \frac{1}{2} g t^2 \tag{3B}$$

where v_r and v_z are the velocity components of the initial velocity v_{erup} of the particles in the directions of radius and height respectively, g is gravitational acceleration and t time. Modelling a ballistic ejecta-dominated eruption requires a defined set of particles being ejected in a certain time.

In our model, the angle of ejection defines the r and z components of the initial velocity (assumed constant). The distribution of ejection angles has been investigated by Chouet et al. (1974). Following their investigations, which give a maximum angle of ejection (measured relative to the vertical direction) of 30° and an angle of maximum ejection – i.e. where most of the material is ejected – of 6°, we assume a Gaussian distribution with a median ejection angle $\langle\alpha\rangle$ of 6° and a standard deviation σ of 9.3° to enable an analytical description of the problem hereafter. Note that in a later section, we re-examine the interpretation of the ejection angle distribution measurements of Chouet et al. (1974) and suggest that these data may also be interpreted as consistent with the jet fallout model.

In the purely ballistic case (i.e. negligible gas drag on the particles), the static description of the resulting deposit (i.e. the deposit shape; a description focusing on predicting mass accumulation at any distance normalised to the maximum mass accumulation) is grain-size-independent. This is because purely gravitational acceleration is independent of particle weight (which, assuming a constant density, is equivalent to size) and thus smaller clasts, which need a longer time to build up a large deposit, require longer observation times of the model predictions to build up the same volume than larger clasts. Following Eqs. 3A,B and inserting the Gaussian distribution of

ejection angles, the range of the clasts r_0 and the probability of a clast landing there, $P(r_0)$, can be expressed as a function of ejection angle α as:

$$r_0 = \frac{2v_{\text{erup}}^2}{g}\cos\alpha\sin\alpha \tag{4A}$$

$$P(r_0) = \frac{1}{\sqrt{2\pi}\sigma}\exp\left[\frac{(\alpha-\langle\alpha\rangle)}{2\sigma^2}\right] \tag{4B}$$

The simulation of this set of equations leads to a deposition trend as in Fig. 4. The closest empirical approximation to the resulting sedimentation trend $S_{\text{ball}}(x)$ by a simple function is a reciprocal curve, i.e.:

$$S_{\text{ball}}(x) \approx \frac{A}{x} \tag{5}$$

where A is a factor which is physically related to clast weight (i.e. also diameter, shape and porosity), gravity and eruption velocity – assuming the latter two define the statistical distribution of ejection angles. The correlation coefficient of the modelled ballistic curve in Fig. 4 to the simple reciprocal function is $\sim$0.99 and shows that deposition by purely ballistic ejection (i.e. no drag) is well approximated by a reciprocal curve.

This result changes significantly once the drag exerted by gas on the clasts is accounted for. Drag changes both Eq. 3A and Eq. 3B because the resistance to air changes the velocity vector:

$$\vec{v}\left(=\begin{pmatrix} v_r \\ v_z \end{pmatrix}\right) \text{ by } \nabla\vec{v} = -\xi\sqrt{(v_r+v_z)}\frac{\vec{v}}{2} \tag{6}$$

where ξ is the drag coefficient, which is given by ($\xi = 3\rho_{\text{air}}/16\rho_{\text{p}}d_{\text{p}}$) following Melnik (1996). So the effect of clast size (here represented by its diameter d_{p}) on the normalised sedimentation trend starts to be important. Integrating Eq. 6 numerically for every time step (stepwise integration by calculating the average of upper and lower Darboux sum; e.g. Kestelman, 1960) results in the grain-size-dependent drag model. Fig. 4 illustrates typical predictions of normalised sedimentation trends for two contrasting input grain-size distributions with Inman sorting of 1 (chosen as this value appears typical for cinder cone deposits; see Table 1 and Fig. 3). Increasingly coarse grain-size distributions show a shift of the deposit nearer to vent as an effect of the higher resistance to gas drag (ζ tends to 0). In contrast to the no-drag (ζ tends to 1) case, the predictions accounting for gas drag are not well represented by a simple reciprocal curve. For small particles ($d < 1$ cm), the best approximation is a power law close to A/x, whereas for larger clasts the best approximation is a function of the form:

$$S_{\text{ball}} \approx \frac{A}{x}\,\mathrm{e}^{Bx} \tag{7}$$

There is now an exponential factor in the function stemming from the large drag. The correlation coefficient is $\sim$0.98. Hereafter in the paper, we will use these approximation curves as representative of the theoretical curves in comparisons with field data.

2.3. Sustained jets

A no-wind model for the deposition from turbulent, pressure-adjusted, momentum-driven jets (and pure buoyant plumes) has been presented by Ernst et al. (1996). We assume that the jet is fully developed directly at the vent, which is reasonable if vent size (r_{v}) is small compared to the extent of the deposit we are modelling.

The equations given for the sedimentation by Ernst et al. (1996) assume a well-mixed, dilute, simple jet expansion and a top-hat velocity profile, i.e. constant across the jet. After accounting for the effect of particle re-entrainment into the jet, their equation 28 for the deposition from a sustained jet can be written as:

$$S_{\text{jet}}(x) = S_1\frac{J_{\text{j}}/x - \xi_{\text{j}}\Phi_{\text{j}}/2\alpha_{\text{j}}x^2}{J_{\text{j}}/r_1 - \xi_{\text{j}}\Phi_{\text{j}}/2\alpha_{\text{j}}r_1^2}\,\mathrm{e}^{-J_{\text{j}}(x-r_1)}\left(\frac{x}{r_1}\right)^{\xi_{\text{j}}\Phi_{\text{j}}/(2\alpha_{\text{j}})} \tag{8A}$$

where α_{j} is the entrainment coefficient, Φ_{j} is the particle re-entrainment coefficient, ξ_{j} is a geometrical factor which depends only on α_{j} (see Ernst et al., 1996), and r_1 is the minimum distance corresponding to the lowermost height where jet flow applies (r_1 is assumed to be equal to r_{v}). Eq. 8A also assumes full sedimentation by the jet. Some

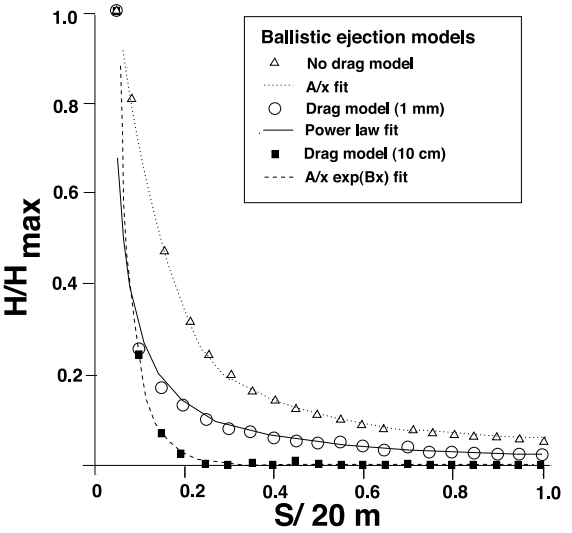

Fig. 4. Predictions of a typical ballistic experiment: The triangles represent the numerical ballistic growth results without drag (200 000 particles have been erupted here). The boundary conditions for the experiments are described in the text. Reciprocal-type curves fit the no-drag ballistic curves best (dotted line, see text). When considering the drag forces on ballistic particles, the grain-size distribution becomes decisive. Numerical experiments were thus conducted with log-normal grain-size distribution with characteristic Inman sorting of 1 and various median grain sizes. These median grain sizes and the symbols used for plotting them are shown in the legend. Clast distributions of the order of 1 cm and smaller, here represented by 1 mm, notably diverge from coarser distributions, here represented by 10 cm. This is also reflected by the best-fit curves to the numerical experiments which are a power law for median grain size of 1 cm and smaller (dashed line, see legend) and a simple function of the type $f(x) = A/xe^{Bx}$ for bigger particles (dashed lines, see legend).

of the particles might be lost to a plume above the jet region. This model description is thus appropriate for plinian-style sedimentation where most of the particles would be coarse enough to fall off the margins of the jet region in the lowermost region of an eruption column. J_j, the constant in Eq. 8A, is calculated from Ernst et al. (1996) as:

$$J_j \approx 0.267 \frac{\xi_j v_t(d)}{4\alpha_j^2 \sqrt{M_0}} \quad (8B)$$

Here, $v_t(d)$ represents the terminal fall velocity of a particle of diameter d. Expressions to estimate the terminal fall velocity of volcanic clasts can be found in Bonadonna et al. (1998). It depends on particle Reynolds number (or drag coefficient) which in turn depends on particle diameter.

The results are shown in Figs. 5 and 6. For the contrasting grain-size distributions illustrated in Fig. 3 and a constant eruption velocity of 50 m s^{-1}, all the deposition trends from the assumed grain-size distributions are similar (Fig. 5). Mass accumulation decreases approximately exponentially with increasing distance from vent. However, in another series of numerical experiments with a given grain-size distribution and contrasting eruption velocities, this seemingly consistent pattern changes once the eruption velocity is increased to values significantly above 50 m s^{-1} (Fig. 6b) for grain-size distributions skewed towards the fines. Near-vent re-entrainment of fine particles becomes so intense that maximum sedimentation which previously occurred at the position closest to the vent (Figs. 5 and 6a) is now shifted towards further from the vent (Fig. 6b). This style of fallout from the jet margin only occurs at very large discharge rates. Those have been measured at volcanoes like Eldfell (Blackburn et al., 1976) and Etna (Cas and Wright, 1987) (see Table 1 for example). However, these volcanoes were reported to have erupted dominantly fairly coarse clasts (see Fig. 5). Thus, the upper graph of Fig. 6 may be representative of the commonly observed sedimentation trend. It is possible, however, that eruptions at high rates and emitting mostly fine clasts (e.g. Lassen Cone; Cerro Negro 1995) contain enough coarse (fluidal) clasts depositing close to the vent (within 10 m or so on either side of the position of maximum deposition) which can weld and preserve the near-vent primary deposition profile. In this case, the vent rim profile is expected to be controlled by eruption velocity and this information could be extracted from accurate measurements of the geometry of the near-vent rim using Fig. 6.

2.4. Spatter cone deposits – frozen deposition trends

One way to evaluate the various model predictions against suitable field data is to look at spatter cones. Falling spatter clasts, in contrast to

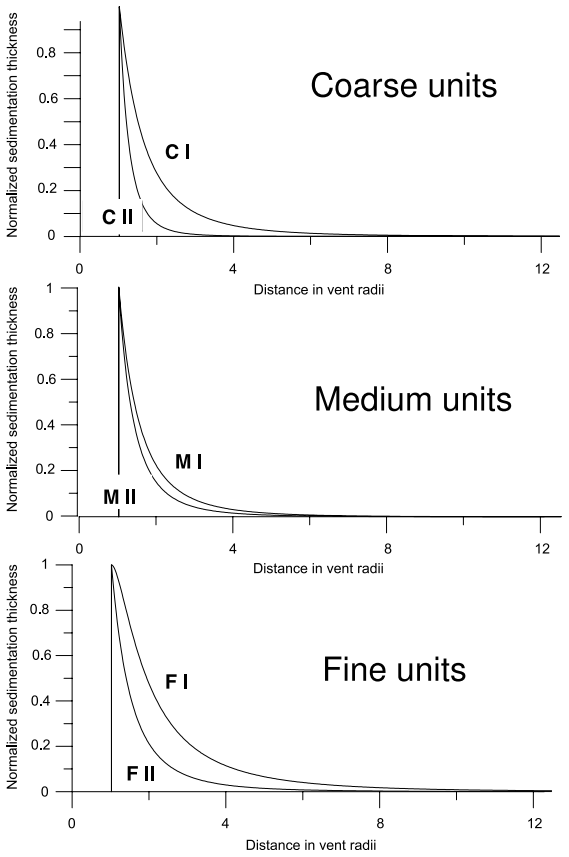

Fig. 5. Predictions of numerical experiments on ejecta construct growth by jet fallout for an eruption velocity of 50 m s^{-1} and a vent radius of 1 m. The jet fallout for various grain-size distributions differs mainly in the distribution towards higher distances for a larger proportion of finer particles. There is a similar general trend, a near-exponential decrease (following Eq. 8) with increasing distance from source. There is only moderate divergence from the overall trend for the 1995 Cerro Negro eruption (curve annotated as grain-size distribution 'F I'), for which the concave curvature becomes convex for the near-vent deposit. At higher eruption velocities this leads to a decisive diversion from the overall trend depicted here at low velocities (Fig. 6b).

cinders, are large and partially molten and retain enough heat to fuse with each other where they land. Secondary flowage is minimal and limited by the constraints of viscous flow and visco-plastic deformation. Observations from photographs suggest that this only affects the near-summit region of the cones.

Here the digitised slopes of the four spatter cones we have examined (see Fig. 2) have been approximated empirically by simple functions. The predictions of ballistic models with and without drag, and those from the jet fallout model may thus be evaluated against the spatter mound data (Fig. 2). Fig. 2 shows that the jet fallout prediction (from a simplified version of Eq. 8A without re-entrainment, as re-entrainment of large spatter clasts is unlikely here) approximates the data much more closely (correlation coefficient $R^2 \sim 0.98$) than the ballistic prediction without drag (Eqs. 5 and 7; $R^2 \sim 0.73$–0.77). The ballistic model with drag is closer to the data trends ($R^2 \sim 0.96$), but the jet model provides a slightly better approximation for spatter mound deposits than the ballistic models. This finding is in agreement with the jet dispersal model of Parfitt and Wilson (1999). The significance of the deviation by 0.02 in the correlation coefficient between the two best-fit models, i.e. for jet and ballistic with drag, however, is doubtful and we will treat the two values as equally good.

Intuitively, the convergence of the ballistic predictions with drag and those of the jet fallout model is to be expected as the jet fallout model is a drag-dominated end-member description with negligible lateral ejection. Figs. 2 and 6a also suggest that the amount of lateral ejection in spatter eruptions is small and does not amount to more than the lateral displacement from vent expected if a clast falls directly from the margins of a conical jet which expands linearly with height (e.g. radial displacement expected at the top of a 50 m or 500 m high lava jet, and corresponding to the furthest dispersal in no wind achieved by a clast, is $\sim$5 and 50 m, respectively).

The slopes of spatter cones – which as stated earlier are assumed here to have frozen states of the sedimentation process – compare more favourably to the sedimentation trends predicted by a sustained jet model than a purely ballistic model.

3. Limitations of the jet fallout model

The jet fallout model that we have presented is only a first-order model. It has some limitations.

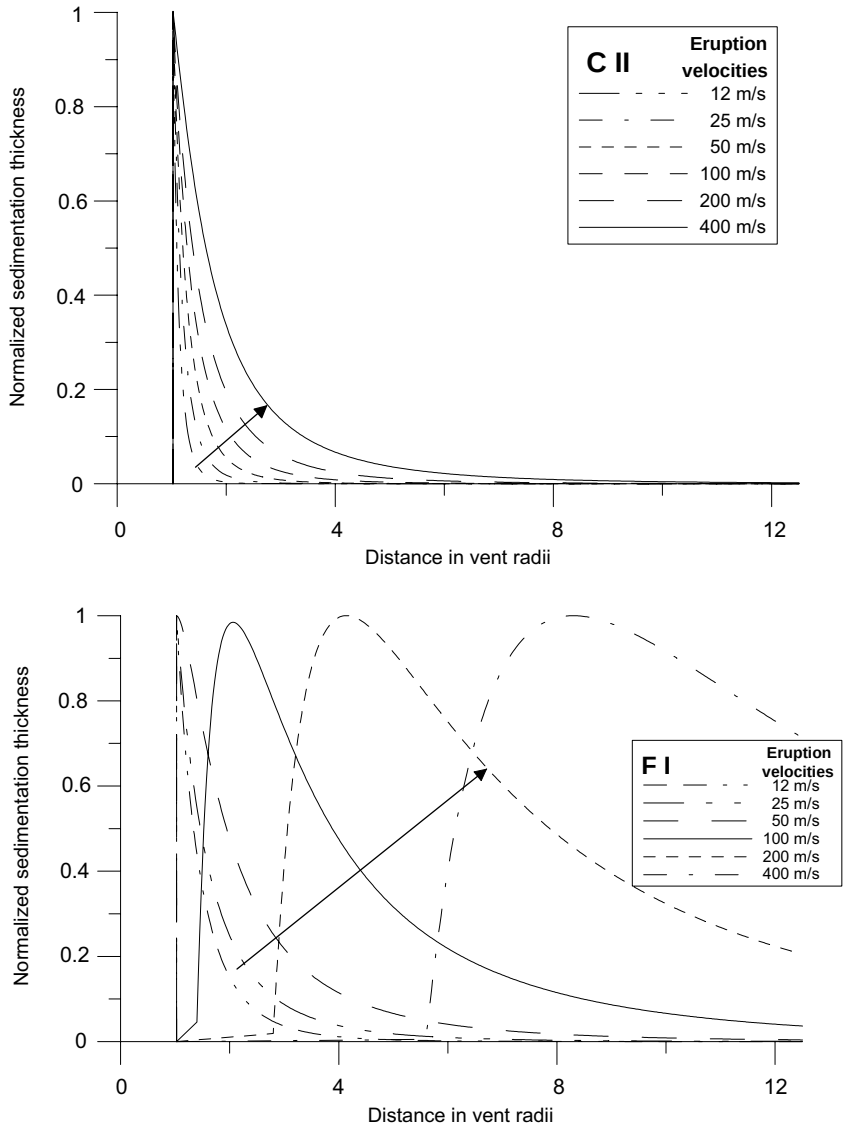

Fig. 6. Predictions of numerical experiments on ejecta construct growth by jet fallout. (a) The upper graph illustrates expected deposition trends for coarse-grained and medium-grained eruptions. As an example, the values for 'C II', i.e. the Etna NE crater, have been selected to illustrate the predicted near-vent eruption thickening at higher eruption velocities. All the curves are overall monotonically concave, in contrast to (panel b) fine units such as that of grain-size distribution 'F I' (modelled after Cerro Negro eruption 1995). At low eruption velocities the curve is like that predicted for coarse-grained eruptions. However, when eruption velocity exceeds a threshold value between 50 and 100 m s^{-1}, the curvature changes from concave to convex beyond the rim. At the same time, the distance to the point of maximum sedimentation increases for increasing eruption velocities.

Here we briefly discuss some of the assumptions of the model and their expected limitations.

We assumed that the jet flow rapidly adjusts to atmospheric pressure. This is only reasonable for moderately explosive events such as those we are considering. The assumption that the flow is dilute is not valid at the vent. However, we envisage that due to the extreme shear, impulsive growth

of eddies at the jet margins and rapid mixing with surrounding air the jet flow will become almost instantly dilute there. Hence this assumption is a reasonable one to make initially.

Further, it has been implicitly assumed that flow density, which is initially higher than atmospheric density, becomes rapidly close to that of surrounding air to within a few percent. This justifies the use of the Boussinesq approximation (see Sparks et al., 1997) in the derivation of the jet Eqs. 8A,B. The fact that pyroclastic flows stemming from high-density contrasts are only rarely and even then only episodically generated during cone-forming eruptions supports our suggestion that density contrasts are rather small.

A further assumption is that jet flow and particle fallout are unaffected by crosswinds. This assumption is only valid in the region of the jet flow where the characteristic velocity is larger than typical crosswind velocity at that level. Many eruption jets are powerful, with velocities higher than 30 m s^{-1} over much of their height so that jet flow is not substantially influenced by winds. Particle fallout will not be much influenced by crosswinds in two situations: (1) if particles fall from relatively low heights so that there is little time for advection by wind over significant distances – we are focussing on the case where the bulk of the particles fall from an eruption jet which is a few tens of metres to a few kilometres in height, so that an effect of wind is expected but is less strong than in the case where one considers fallout from much higher up in an eruption column; (2) if particles are relatively large and coarse, of the order of 1 cm or more, the effect of crosswinds will be moderate – a median size of 1–4 cm is the characteristic size for many ejecta cones so it seems that there will be an effect of winds but that it may be moderate. Thus, in summary, it is clear that we presented only a first-order model.

4. Effect of early spatter mound phase or pit crater formation on cinder cone morphometry

A morphological cause of deviation from the constant PW ratios of cinder cones (0.4) needs to be briefly discussed, which is related to typical spatter cone phases and which accounts for the natural variability in reported values of cone aspect ratios. Avalanching in ejecta cones can take place toward the internal cone base until the vent is blocked or the eruption stops. If, however, the ejecta cone is built on top of a spatter mound the avalanching baseline is elevated. Because a spatter mound is welded, it does not allow internal drainage towards the cone base, but elevates the vent, often filled with a small lava lake, at the top of the welded spatter mound. This can change the PW width ratio of Eqs. 1 significantly (Fig. 7a). The height of the internal spatter mound, H_{spatter}, can be estimated if baseline elevation is the cause of divergence between measured ratios of W_{cr} to W_{co} and the constant 0.4 ratio of Eqs. 1. Using the method of similar triangles (Fig. 7a), we note that:

$$H_{\mathrm{spatter}} = H_{\mathrm{co}}\left(1-\frac{3W_{\mathrm{cr}}}{4(W_{\mathrm{co}}-W_{\mathrm{cr}})}\right) \quad (9)$$

Because spatter mounds usually do not appear to grow beyond a height of 30 m, the relative effect on ejecta cones much higher than 30 m (e.g. cinder cones such as Paricutín can reach heights up to 400–500 m) should be small. This seems to be the case in the studies of Wood (1980) and Carn (2000). In the study of Bemis (1995) cones with strong deviations are also found for large crater heights. Examples in Table 1, where an underlying spatter mound may affect the aspect ratio significantly, may include the Navidad Cone at Lonquimay (Chile; Global Volcanism Network, 1989) and Kapoho (Hawaii, from visual observations; Richter et al., 1970). Spatter cones can only account for a smaller ratio of W_{cr} to W_{co} than 0.4. Similarly, as illustrated in Fig. 7b, cinder cones developed above a deep pit crater are expected to have ($W_{\mathrm{cr}}/W_{\mathrm{co}}$) values larger than 0.4, i.e. a wide crater, which seems to be fairly typical for the beginning stages of the Laghetto cone during the Etna 2001 eruption (Calvari and Pinkerton, 2002; Pfeiffer, 2001) and a good explanation for the variation in Bemis' study (1995), where maars are relatively frequent in the survey area.

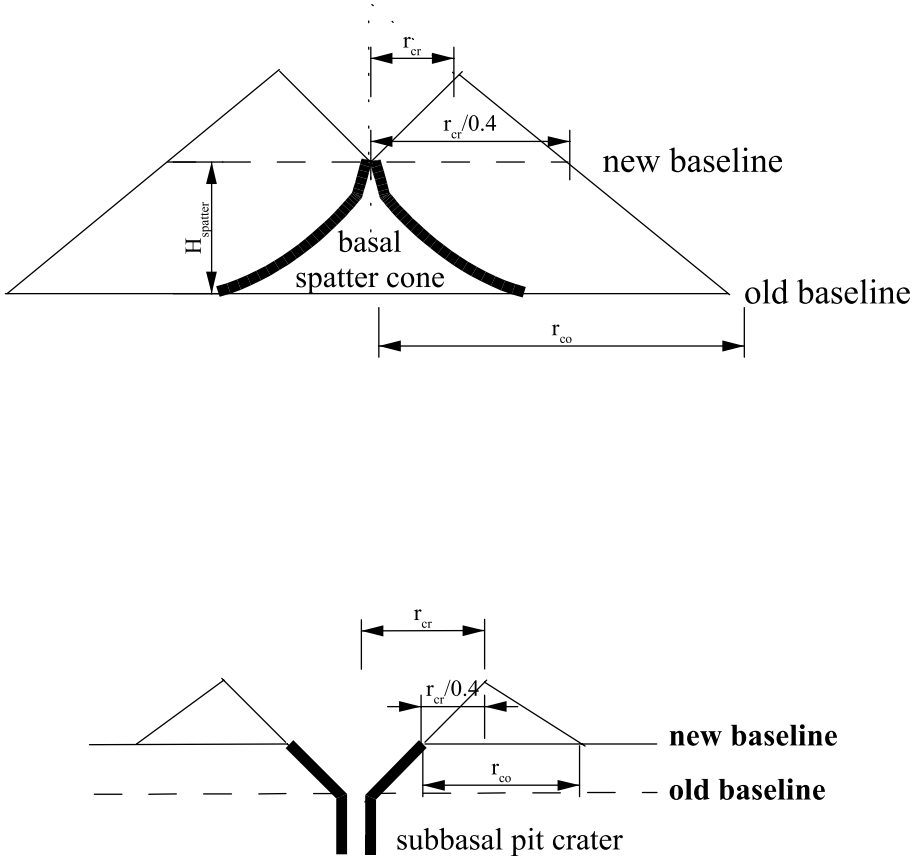

Fig. 7. Sketches illustrating possible causes of deviation from the 0.4 widths aspect ratio in freshly erupted ejecta constructs (here sketched as a cinder cone for simplicity). (a) Effect of an underlying spatter mound. The inner crater avalanching is elevated by the presence of an underlying spatter mound which grew in the opening phase of eruption. The method of similar triangles can be used to determine the height of the spatter cone from these apparently overly high cinder cones. (b) Effect of a pit crater on the ejecta cone aspect ratio. Equally, the presence or development of a pit crater can account for deviations from the 0.4 aspect ratio value. See text for details.

5. Grain pile laboratory experiments to model ejecta cone slope and crater formation

5.1. Motivation

The jet model can only account for formation of a crater rim offset from the vent for high eruption velocities and a fine-grained erupted size distribution (Fig. 6). In this case, the point of maximum sedimentation (PMS) is not at the vent and the crater rim of an ejecta cone may correspond to the PMS. Rim growth is clearly observed to occur during cone growth rather than post-eruption (Wood, 1980; Magus'kin et al., 1983; Tokarev, 1983).

On the one hand, the vent-offset crater rim could be accounted for using a jet model with rising velocities at the vent, because from Fig. 6 it can be clearly seen that crater rim radius is dependent on eruption velocity. However, at least two lines of evidence may not be in favour of this hypothesis: (1) this appears inconsistent with aspect ratios for many hundreds of young cinder cones – if changing eruption velocity was the primary control on rim position, one would expect a much larger range of aspect ratios than has been reported (e.g. Wood (1980)). Note, however, that Bemis (1995), on the basis of morphometric measurements of cones in Guatemala, argues that such a large range of aspect ratios does

indeed exist in at least some cone fields; (2) observations of normal grading in ash blankets associated with at least some cinder cones suggest decreasing rather than increasing eruption intensity with time, or eruption intensity decreasing within each explosive pulse contributing to cone growth during strongly intermittent phases. However, to our knowledge, there has not been a systematic study of grading in cinder cones so that one should be cautious of ruling some factors out prematurely.

On the other hand, once loose tephra is deposited, avalanching typically follows immediately. Slumping in the crater is frequently observed during cinder cone eruptions as a syn-depositional process (Verwoerd et al., 1981; McClelland et al., 1989), and may be expected to play the primary role in controlling the position of the crater rim. For eruptions where the PMS is always at the vent edge, i.e. for which low-velocity jet fallout or ballistic ejection with drag may account for deposition, surface grain flow avalanching appears to be the only mechanism which can account for the development of a large vent-offset crater rim with 0.4 width ratio, steep inner crater slope and crater rim position where it is observed.

For more intense eruptions, an expectation may be that repeated explosions keep clearing the vent and inner crater slopes at intervals (as suggested by Wood, 1980), forcing the uppermost material at the surface to remain in motion, as it would in an experiment where material is drained centrally from a conical pile made up of loose (low-cohesion) granular material. Such experiments, illustrating cone pile drainage with concentric avalanching, are presented next, following a brief review of the relevant granular pile mechanics. The laboratory experiments, developed with volcanic cones in mind, complement the numerical modelling and experiments, and further explore controls on ejecta cone geometry and aspect ratios.

5.2. Review of grain pile mechanics

A grain pile builds up continuously until its slopes reach the *angle of repose*. If further grains are piled on top, avalanching will control the growth process. The angle of repose is a material constant, but is rather loosely used as pointed out by Miller and Byrne (1966): as either (1) the angle at which a single grain starts to tumble down a tilted layer, a *dynamic* definition, or (2) the angle at which a grain pile is at rest (Van Burkalow, 1945), a *static* definition. In microscopic terms these angles correspond loosely to the *angle of internal friction* and the *maximum angle of stability* (Oda and Iwashita, 1997). Rock material reacts in a different way to static and dynamic friction. It is easier to overcome dynamic than static friction, i.e. it is easier to keep a system moving than to initiate first motion. If a system is not moving, any force must first overcome its static friction. A geological analogue behaviour is observed during earthquakes. Since static friction is not always overcome, large stresses can build up along seismogenic zones, that will more easily break the material than get it into motion. The initial fracturing process reduces the static friction, however. Further movement along the initial fracture can then occur against its lower dynamic friction, which allows a build-up of stresses to produce aftershocks (typically less intense than the initial earthquake).

Further insights are gained from work in granular flow mechanics related to the development of agricultural storage containers. Here, even the static angle of repose is considered an ambiguous term and thus a distinction is made between the *emptying* (or 'concave') *angle of repose* which develops on granular material drained through an underlying gate – while a crater is forming inside the container – and the *filling* (or 'convex') *angle of repose*, i.e. the slope of the pile growing on a flat ground surface underneath the gate (Kammel, 1997).

Thus, the three different angles under consideration here are the *dynamic* angle of repose, and the *emptying* and *filling* angles for formations at rest. Generally, the emptying angle is steeper than the filling angle (Kammel, 1997). We anticipate that cinder cones at rest might exhibit these two different slopes: the filling angle on the outer slope and the emptying angle inside the crater.

All three angles of repose have been investigated for sand piles. By its tectosilicate nature

(and thus roughly similar density to that of volcanic glass, e.g. as in scoria), loose granular nature, angular shape and moderate sorting, natural sand can serve as a useful analogue for pyroclasts and/or ash making up ejecta cones. Whereas Miller and Byrne (1966, and references therein) made the experimental investigation of the dynamic angle of repose, Van Burkalow (1945) investigated the filling angle by looking at angles of sand piles at rest. The emptying angle is the common angle observed in the so-called *draining crater method* (Brown and Richards, 1970), where a sand container is emptied through a hole at the container's base. The remaining crater after drainage is believed to be at the angle of repose, and equal to the *emptying* angle (at rest). For sand, the *filling* angle was observed to be 34° (Bagnold, 1941) and should, for spherical particles, lie at ~30° (Barabasi et al., 1999). For cinder cones the ratios of equation 1 of Wood (1980) imply a similar angle of ~31°.

5.3. Experimental setup

In order to test the hypothesis that cinder cones are shaped by the same forces as small-scale grain piles, we conducted laboratory experiments. The setup (Fig. 8) consisted of a flat, square, wooden board (400 mm×400 mm) with a 10 mm diameter, circular outlet located at its centre and initially plugged by a sponge cork attached to a 1 m long string. At some low height (30–120 mm), which was adjusted for a given run as a function of the size of the cone to be built above the centre of the flat board, a large plastic funnel with a long and narrow neck filled with fine, dense angular, and low-cohesion (dry rather than moist) grains, and initially closed at its lower outlet was placed, held firmly in position by a support system.

The granular material in the funnel was then allowed to flow downwards and to accumulate grains over the flat board. This arrangement produced a steady supply of grains to the board (steady supply is imposed by the high frictional resistance of the long narrow neck walls to sand flow, which buffers flow rate to a constant value), and formed a conical grain pile within a few tens

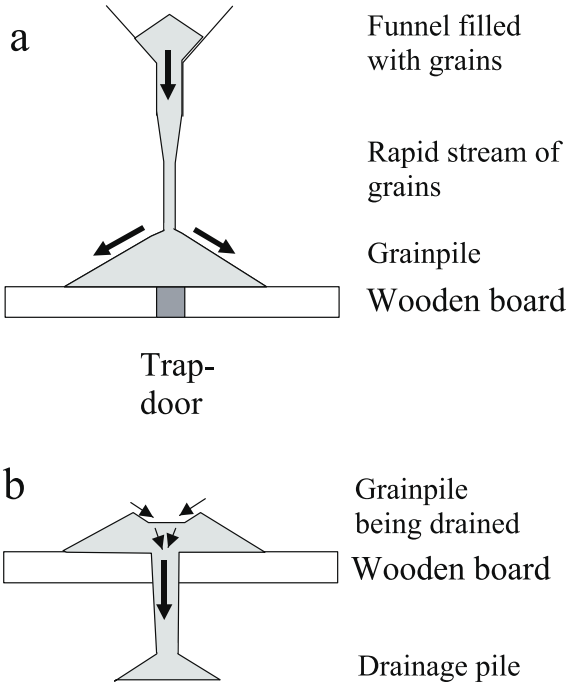

Fig. 8. Sketch of the experimental setup used to investigate processes involved in cone and crater development and controls on ejecta cone aspect ratios. (a) The setup consists of a wooden planar board with a central drainage orifice which is initially plugged by a sponge cork. The board serves as a baseline for the growth of a granular pile supplied by a steady flux of grains from a long and narrow funnel (not to scale). The arrangement is such that the pile's apex is located above the drainage orifice. (b) Whereas the first part of the experiments allows one to examine processes involved in pile growth, the second part allows the examination of crater development. The drainage orifice is then quickly opened up to form an inner crater to the pile. The drainage products are evacuated underneath the drainage orifice.

of seconds (Fig. 8a). After the grain pile had apparently come to rest, the board was gently tapped to ensure that it was indeed at rest and thus that its slope lay at the filling angle. The narrow outlet in the board (outlet centred below the cone apex) was then quickly opened up (Fig. 8b), allowing the granular material to drain through the outlet and resulting in formation of a central depression of inversely conical geometry and inner slope steeper than the outer slope of the initial cone. Beyond a well-defined circular rim, the geometry of the initial cone remained unaffected by crater formation. After the inner crater

slope had reached a state of apparent rest, the board was again gently tapped to ensure that it indeed had reached its equilibrium slope.

Materials used as a source of grains were either sand ($\sim$0.5 mm median grain size and rounded), sugar ($\sim$1 mm median grain size and cornered), flour ($\ll$100 μm) or mixtures of various proportions of these to evaluate a possible dependence of the results on the system's mechanical scale. To examine dependence of the results on system size (i.e. height of cone or volume of material used), piles of varied base diameters were allowed to develop in successive experiments (Table 2). After each run, the height of the crater rim above the cone base (H_{co}), the distance r_{cr} from the central hole to the crater rim and the distance r_{co} from the central hole to the outermost grains within the pile were measured (Table 2).

Scaling aspects (illustrated by the case of sand piles) are considered next and followed by a presentation of the key observations and data from the new experiments.

5.4. Scaling considerations

Our laboratory model is typically a sand pile with a base of the order of 0.1 m radius (Table 2). Volcanic cinder cones possess a base radius of the order of 100 m, so the geometrical scaling is about 1:1000. In order to obtain a correct mechanical scaling of our laboratory model, the dynamic similarity between our laboratory model and cinder cones is also required. The fundamental dynamical relationship of relevance here expresses how shear strength τ, i.e. the resistance to shear of the medium, and applied shear stress, σ, are related (Coulomb, 1773):

$$\tau = c + \sigma \tan \Phi_f \quad (10)$$

where c is cohesion and the second term is the friction term, which is a product of σ, stress, and Φ_f, the filling angle. Stress σ on each grain arises from the other grains pressing on it from a higher potential energy level. In the presence of gravity the energy of a particle at rest is defined by its weight. Since avalanching is equivalent to the state that this force overcomes the friction, we need to find the most likely point where this occurs. That is clearly the case where the loading by the other grains is at a maximum. This is calculated as the product of material bulk density (particle density ρ_p, multiplied by the average particle volume fraction ϕ, which is related to voidage and packing arrangement), gravity g and the length scale, which is given by h, the pile thickness (also directly proportional to cone diameter):

$$\sigma = \rho_p \phi g h \quad (11)$$

For a pile of grains of roughly the same size (moderate sorting), particle volume fraction in the pile, ϕ, is in the range between 2/3 and 3/4 (e.g. Allen, 1985), and will be roughly in the same range in natural cones.

With h being scaled 1:1000, ϕ being scaled approximately 1:1, and ρ_p being scaled about 2:1 (for average sand particle density of 2700 kg m^{-3} and pyroclasts averaging half of this), we model a stress of 1:500, since gravity is the same for the lab model and cinder cones. Rocks and sand share a common range of filling angles (25°–40°; Handin, 1966), so that the friction term translates directly into shear strength with the same scaling. Cohesion has been measured for natural cinders at about 200 kPa (Bowman et

Table 2
The cone and crater forming experiments for sand and sugar cones listed in the table are illustrated in Fig. 12

Material	r_{co} (cm)	r_{cr} (cm)
Sand	6.2	2.9
Sand	13.5	6.5
Sand	14.1	6.4
Sand	21.2	8.0
Sand	22.5	9.9
Sugar	8.5	3.8
Sugar	8.7	3.8
Sugar	11.9	5.3
Sugar	14.9	6.5
Sugar	15.4	6.5
Sugar	16.0	7.5
Sugar	19.4	9.4
Sugar	20.9	9.5
Sugar	22.4	9.6
Sugar	25.4	10.4

The vent radius r_v of the experiment was 0.5 cm, which has to be and is not yet subtracted from the cone radius (r_{co}) and crater radius data (r_{cr}) to coincide with the values in the figure.

al., 1998). So an analogue laboratory granular material would be adequate if its cohesion is in the range of up to 400 Pa (i.e. if the c term in Eq. 10 is about an order of magnitude less than the $\sigma \tan \Phi_f$ term in both the ejecta and experimental cones). Dry sand or dry sugar have cohesion values of this order (Handin, 1966) and are thus suitable analogue materials for loose pyroclasts in cinder cones.

5.5. Observations, data and basic interpretation

In the experiments using sugar or sand, the processes observed are very similar. While the pile is growing, the grains build up on top of the existing slopes until the dynamic angle of repose is exceeded, which is very early on in the experiments. Then the grains either roll down individually or move down as part of surface grain flows involving many particles, and spreading symmetrically downwards from the top of the pile (axisymmetric grain flow occurs only when grain supply flux exceeds a threshold value). The axisymmetry is broken if the funnel is not held sufficiently firmly or exactly positioned above the top of the growing pile, and data from these experiments were discarded. The avalanching is best visible in experiments using a mixture of sugar and sand, because the sugar particles are larger than the sand particles. Spontaneous stratification quickly develops. The sugar grains are transported preferentially to the top and front of the surface grain flows and wave after wave the fronts of the surface flows are readily visualised. Under the steady flow conditions imposed by the funnel source, the surface grain flows follow each other in equal time steps.

Once the outlet centred below the pile's apex is opened up, the grains drain through the underlying opening, until the forces of static friction overcome the decreasing dynamic forces of avalanching (see Fig. 9). Finally, the emptying angle is reached. On the steeper slope of the rapidly developing inner crater, the surface grain flows move faster than during the pile-building stage and segregation is more extensive. The sand and sugar avalanches appear to form separately, from the pre-established spontaneously stratified alternating strata of sugar and sand grains. Segregation is enhanced on the steep slope of the inner crater by rapid granular flow, where grain–grain collisional effects become important relative to the grain–grain friction effects (in contrast to the pile build-up stage). If pure sand or pure sugar is used, grain flow avalanching does not occur from alternating strata and thus seems to be more continuous. The constructs produced in the experiments, however, share a constant geometry irrespective of whether sugar, sand or a mixture of the two is used. A conical pile-crater as-

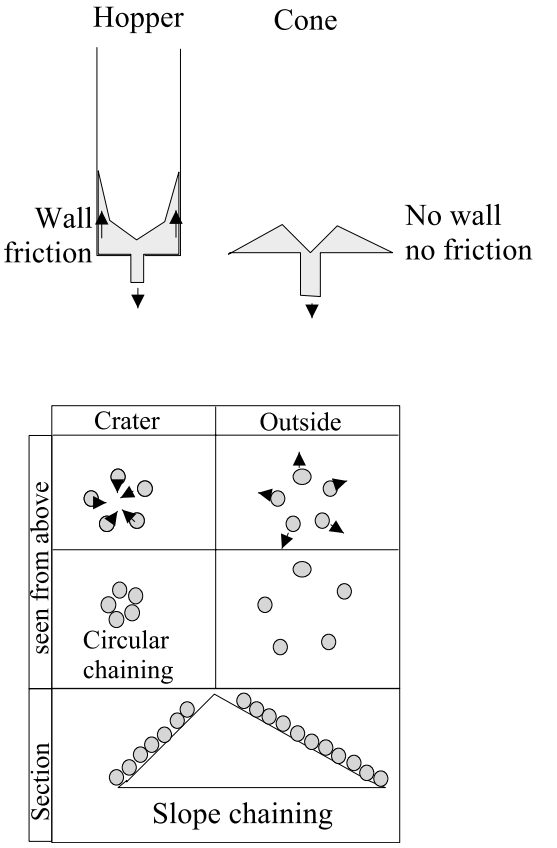

Fig. 9. Sketches illustrating the inter-particle forces active in the experiment. The wall friction effect of hopper drainage experiments is not an important effect because a free surface to the cone develops. The cone slopes are stabilised by the chaining friction force between grains. Slope chaining develops because particles cannot roll one over another once the angle of repose is reached. Circular chaining exists, because the finite size of the particles does not allow them to occupy the same space once they move towards each other.

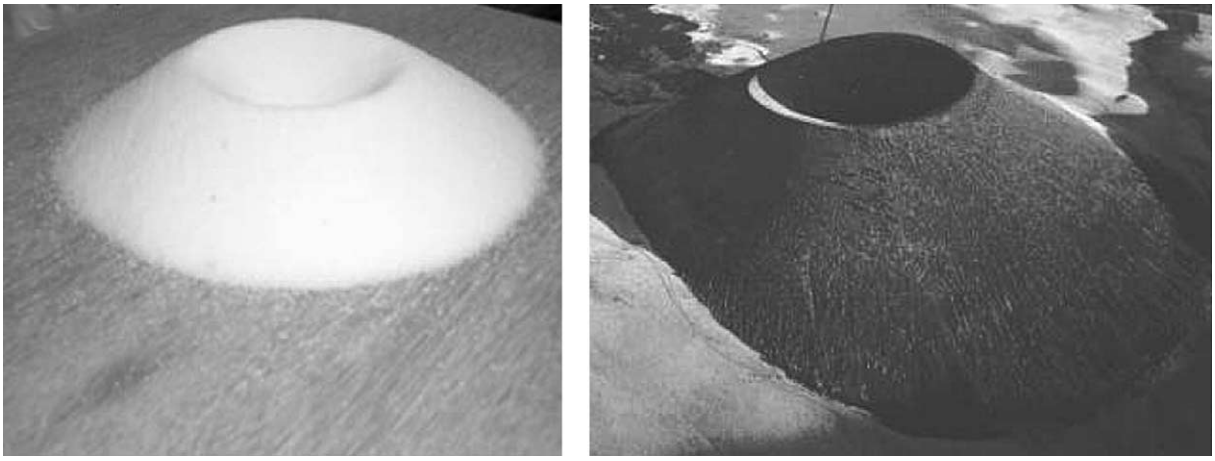

Fig. 10. The similarity between (a) a drained sugar pile, created by the grain pile experiments (see text) and (b) a real cinder cone (here SP crater, Arizona) is readily visible. A more quantitative comparison is shown in Fig. 11.

sembly grown in a typical experiment is presented in Fig. 10a.

The outer slope angle was observed to be 28°–30° for pure sieved sand (relatively fine-grained), 33° for sugar (relatively coarse-grained) and 28°–32° for mixtures of the two. The inner crater angle was in the range 42°–46° for all the experiments with only sand and/or sugar. All angles were measured using a protractor. The resulting radii of crater rim r_{cr} and cone base r_{co} are presented in Table 2 and illustrated in Fig. 11. The ratio of r_{cr} over r_{co} for sugar and sand is remarkably constant. The best linear fit through the data passing through the origin for the pure sugar and pure sand experiments shown in Fig. 11 is given as:

$$r_{cr} = k r_{co} \tag{12}$$

where $k \approx 0.43$ for pure sugar and $k \approx 0.42$ for pure sand.

Spontaneous stratification, which was observed during the sand/sugar-mix experiments does also occur in natural cinders of different sizes, as has been shown by Bemis and Bonar (1997). The results obtained for the spontaneously stratified sand–sugar piles thus add the insight that having grains of different sizes and densities in the laboratory cinder cones does not appear to affect the crater-and-cone overall aspect ratios noticeably.

Another series of experiments was then carried out to gain insight into the control on cone aspect ratios of increasing cohesiveness within the deposited material. The experiments were developed with volcanic cones with increasing amounts of fine (typically also wet) ash in mind. In this series of experiments, much finer, cohesive particles of flour were added to either sand or sugar, in increasing amounts for successive runs.

Typical grain pile assemblies grown for mixtures of flour, sand and sugar are shown in Fig. 12. The more flour is added to the starting sand/sugar mixture, the steeper the outer slope and inner slope become (Fig. 12). While the pile is forming, the particles are either rolling down individually or moving in bulk as part of surface grain flows. Flour particles which are cohesively clumped together as well as the largest sand particles tend to roll down to the front of the flows, whereas small individual flour particles fall in between the (bigger) sand particles (kinetic sieving effect) and move as part of surface grain flows.

Once the crater is drained, however, the small flour particles stick together and tend to prevent surface grain flow motion. Instead of this, large blocks loosen up from the crater walls along segments of concentric fractures (with spacing dependent on cohesion, i.e. flour amount) and slide down. During sliding, the blocks fragment into smaller blocks, which then slump or roll down and disappear through the hole at the base of the experimental crater. Blocks successively loos-

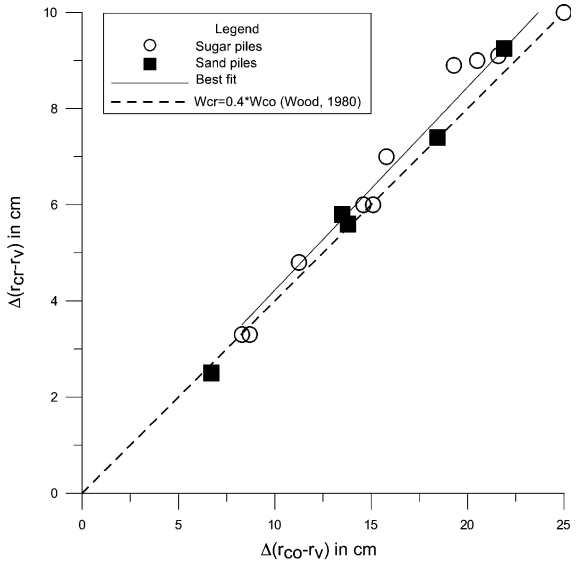

Fig. 11. Comparison of widths aspect ratios for experimental and cinder cones. Assuming vent size is negligible, the difference $r_{cr}-r_v$ is half the distance W_{cr} measured in a cinder cone (Fig. 1) and $r_{co}-r_v$ is half the distance W_{co} (Fig. 1) measured for cinder cones. The ratios for truncated and drained cones produced in the experiment with sand (■) and sugar (○) overlap closely the characteristic ratios for cinder cones (dashed line) found by Wood (1980). Even the best linear fit (thin line) through the origin is close to the cinder cone trend. The error made in measuring the cones in on the order of 1 mm, i.e. smaller than the symbols used.

en up along adjacent segments of the same concentric fault until the entire volume bound by two subparallel concentric faults has been sampled. Then motion along the next concentric fracture accelerates and new concentric fractures grow so that concentric volumes are repeatedly sampled in quick succession, thereby widening the crater. This happens until a metastable angle or state is reached, i.e. metastable because gentle tipping of the board can easily refracture the crater rim and result in an additional slide or series of slides.

5.6. Physical analysis

In the terminology of granular mechanics the *emptying angle* is identical to the angle of the upper boundary of a stagnant zone or discharge angle Φ_d in a cylindrical hopper. Tüzün and Nedderman (1982) proposed that this boundary coincides with an internal failure zone, which opens up between the directions of main stress (Oda and Iwashita, 1997). The typical angle is:

$$\Phi_d = 45^\circ - \frac{\Phi_w}{2} \tag{13}$$

where Φ_w is the angle of wall friction of the hopper. Tüzün (1979) observed angles up to 45° if the edge effects created by the hopper wall friction are weak (e.g. in large-diameter hoppers). In our ex-

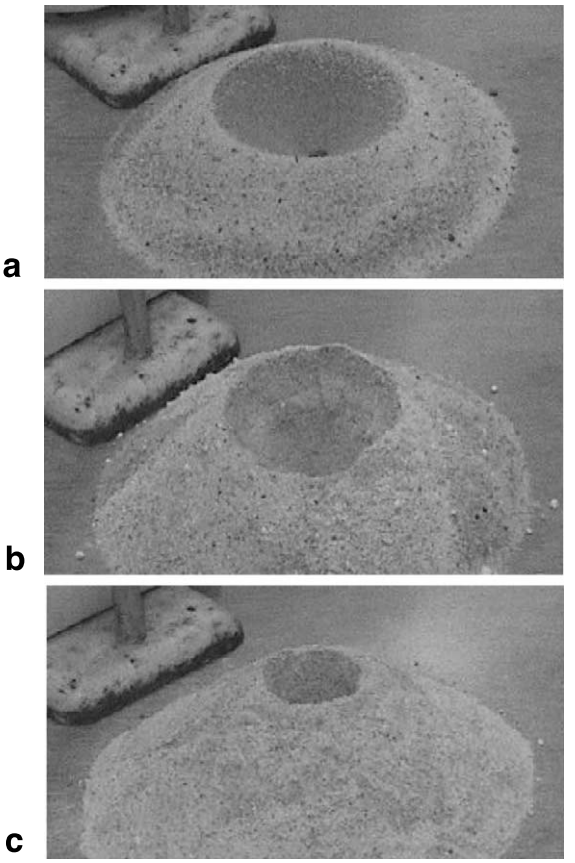

Fig. 12. Photographs of granular constructs grown in experiments, from mixtures of sand and sugar with increasing amounts of added flour (a: 0%, b: 15% and c: 30% flour, respectively, from top to bottom). The crater steepens and becomes smaller with increasing amounts of fine high-cohesion particles such as flour. The outer angle of the construct also gradually becomes steeper when increasing amounts of flour are added. During construct growth for runs with increasing amounts of flour, particle motion also evolves from loose grain avalanching controlling inner crater slope to slumping of walls and falling grains (*ratholing*).

periments, there are no large edge effects as in hoppers because the grain pile is not laterally limited by any vertical rigid boundaries. In the limit case where edge effects are small and can be neglected (wall friction angle of 0°) an inner crater slope at 45° is predicted by Eq. 13 and appears very close to inner crater slopes we measured in our pile drainage experiments.

There is also another way of thinking about this problem. Coulomb calculated the angle of a stable fracture in a layer behaving as a brittle solid, in his so-called *method of wedges* (Coulomb, 1773) as:

$$\Phi_s = \arctan\left(\tan\Phi_f + \frac{1}{\sqrt{2}\cos\Phi_f}\right) \quad (14)$$

For a filling angle Φ_f (i.e. the external slope of a cone of loose granular material) near 30° this gives a stable fracture surface at 45°. A stable fracture can only be created along a stable surface. This requires that the slope surface of the crater inverse cone is stable. Stability can be provided by the increasing degree of grain–grain friction which is inevitable as the particles approach the drainhole. This effect, illustrated in Fig. 9, is sometimes referred to as *circular chaining*. Circular chaining develops in addition to the support of grains along the cone outer surface caused by static friction at the angle of repose (called *slope chaining* in Fig. 9), thus creating a 3D-support for the inner crater slope which contrasts with the 2D-support on the cone external slope. The development of 3D-support in this context has the same final result as would result from grain–grain 'interlocking' that can be achieved by compaction or cementation in another context, for example during the formation of a solid. This is probably why Coulomb's analysis, which was developed for isotropic brittle solids, appears to apply here.

In contrast to isotropic solids, however, where cohesion plays a minor role, because the shear strength is dominated by the main stress field, inter-particle cohesion can become the dominant effect in granular piles and prevent movement initiated by the macroscopic stress field. In the series of experiments where increasing amounts of flour are added, resistance to motion is increased because of the small size and cohesive nature of the flour grains. In granular materials cohesion is created by chemical or electrical bonding. In the case of flour within the mixture, the internal slope collapses concentrically rather than radially and downward by continuous surface grain flows. This effect is often termed *ratholing* in granular mechanics and stabilizes slopes higher than the angle of repose because the material has a substantial yield strength.

6. Comparison between laboratory and volcanic cones

Fig. 10b shows a typical cinder cone (SP crater in Arizona). It closely resembles the experimentally grown pile-crater assembly of the sugar and sand experiments (Fig. 10a). Quantitatively, the ratio of W_{cr} to W_{co} for cinder and laboratory cones is remarkably similar (Fig. 11 and Table 2). The error made in modelling the cinder cone slopes by the experiments is $\sim$5% (0.42 for sand and sugar compared to 0.4 for cinder cones), if we assume that the 0.4 cinder cone width ratio is known exactly (however, the errors of measurements of cinder cone ratios are much larger than the difference between our laboratory measurements and the 0.4 value taken as representative for cinder cones; see Wood, 1980). The difference in laboratory and volcanic cone ratios is sufficiently small to conclude that the angles of repose for emptying and filling are also fundamental controls on cinder cone geometry and that surface grain flow avalanching is the primary control on cinder cone geometry during cone growth.

The observed crater slopes in the experiments with added flour are strikingly analogous to the steep slopes in collapsed tuff cones such as Cerro Colorado, New Mexico, or the inner crater slopes of ultraproximal cones, i.e. cones built by finer particles originating from either hydroclastic or dry-plinian fragmentation. Instead of continuous surface downward motion of loose grains, sliding of blocks occurs and tends to plug up the vent. The metastability of the inner crater slopes becomes important in hazard analysis because piling material at the crater edge which can later fail,

collapse, slide/slump into the vent and plug it, may lead to a premature end of the ongoing phase of activity and/or to the development of overpressure, which may subsequently lead to powerful and hazardous vent-clearing events preceded by little warning.

Some of the above-mentioned effects may account for the gradual vent plugging on January 5–6 1989 during the cone-forming eruption at Lonquimay (Chile), following phreatomagmatic phases erupting fine cohesive ash and then a decrease in eruption rate (i.e. moving into a phase where vent clearing is not a continuous process) – followed by a vent-clearing phase which produced renewed eruption column activity after a gap of some hours; and then again a vent-clearing phase accompanied by increasing seismic activity and strong shocks on January 8th 1989 (Global Volcanism Network, 1989). We suspect that cycles of vent plugging and violent clearing phases following inner cone failure are common, but this has not been reported or studied systematically.

7. Wider implications for field data collection strategies and hazard assessment

Whereas McGetchin et al. (1974) emphasised the ballistic model of volcanic cone growth and the intermittent nature of such eruptions, we have emphasised an eruption jet fallout model of cone growth. In practice, it is likely that both approaches have value. Cone-forming eruptions are more intense in their opening phase than depicted by McGetchin and coworkers, but an intermittent style of activity does tend to gradually become dominant in later stages. Cone growth by ballistic emplacement will be much slower than we have considered here but may go on for months or even years. We expect both mechanisms to significantly contribute to cone growth.

There is a need for modelling how long cone growth activity spends in one phase or the other. Unfortunately, despite frequent cone-forming eruptions, intermittency has not been studied systematically or quantified in any useful way for modelling. Further progress in cone growth modelling requires that such data be collected in future for a number of eruptions so that variability and controls on intermittency can be documented quantitatively and compared with new theoretical models. Time intervals between vent collapse and vent-clearing episodes need to be systematically measured and reported so that modelling of collapse–vent-clearing cycles can be considered with improved hazard assessment in mind in future.

Equally, the total erupted grain-size distribution for eruptions that build up ejecta cones has not been reconstructed (with one exception: see Parfitt, 1998). Here we have had to use proxy grain-size distributions based on analyses of very few samples which are not necessarily representative of a whole cone or a whole cone-plus-ash-blanket erupted. Again, there is a need for these data to be collected in future. In addition to allowing us to learn about the relationship between conduit flow and fragmentation processes and the particle sizes produced, the increasing realisation that cone-forming eruptions can be more hazardous than commonly realised justifies efforts to develop forward models of ejecta dispersal for cone-forming eruptions, as well as models of associated hazards and risks. Finally, the geometry of tuff constructs does not appear to have been quantified. Tuff constructs have readily been classified as cones, although, from theoretical insights, one would expect them to divert from true conical geometry. The slopes of tuff constructs need to be photographed and digitised in future and compared with model predictions for the growth of these constructs. More generally, quantitative data on thickness or grain size of beds in tuff rings or tuff cones collected at increasing distances from vent, are virtually non-existent, and currently there is no suitable dataset to enable comparison with theoretical models of deposition from pyroclastic density currents. This will be the subject of follow-up studies.

8. Closing statements and conclusions

Not all pyroclastic ejecta ‘cones’ actually have a true conical geometry. A systematic review of pyroclastic ejecta constructs and their deposit features, and of observations of eruptions that

form the near-vent constructs, makes a compelling case that many constructs appear to form rather quickly, during events that are more intense and hazardous than has been commonly realised.

Numerical experiments, based on a first-order model of fallout from the margins of an eruption jet, suggest that both cinder cones and ultraproximal plinian cones can be accounted for by the model. The results are consistent with the view, suggested by Parfitt and Wilson (1999), that hawaiian lava fountains can be thought of as plinian columns with a grain-size distribution so coarse that particles cannot transfer their heat fast enough to entrained air to generate a strong buoyant plume into which the particles could be partitioned.

In a plinian column, over 90% of the particles are finer than 1 mm so that heat is efficiently transferred to entrained air, forming a powerful buoyant plume into which almost all the particles are partitioned. The low proportion of particles that do not make it to the plume falls from the eruption jet and builds up an ultraproximal ejecta cone that merges laterally into the plinian sheet of fallout accounting for most of the erupted volume of plinian deposits. In many 'strombolian' or 'violent strombolian' eruptions, both a 'hawaiian' lava fountain and eruption jet, and buoyant plume region coexist, but a greater proportion of the erupted particles fall out from the lava fountain and eruption column jet region than in plinian eruptions, thus resulting in the formation of thick cones and of thinner, albeit extensive, fine ash blankets which are often overlooked due to their poor preservation potential and inconspicuous nature.

Bonadonna et al. (1998) suggested that plinian fall deposits are expected to show four segments on diagrams of log (thickness) versus square root of the enclosed isopach areas. These segments have been related to fallout of large clasts from the vertical eruption plume and of large, intermediate and small particles from the umbrella cloud corresponding to three distinct Reynolds number settling regimes. Such diagrams are important in volume estimation of deposits and also because the slope of each segment contains information on key dynamical parameters. Here, we now anticipate the existence of a fifth segment, an ultraproximal segment. Deposits corresponding to the column fallout segments have been noted in some studies but dismissed as being the result of ballistic accumulation (e.g. Fierstein and Hildreth, 1992; Hildreth and Drake, 1992). Here we propose that the most proximal segment corresponds to eruption jet fallout and the development of an ejecta cone around the vent.

In cinder cone- and ultraproximal plinian cone-forming eruptions, the numerical experiments do not allow us to test the model predictions directly because the primary dispersal of mass is immediately modified by surface grain flows. The model principles were, however, successfully tested by comparison with data for some of the largest spatter mounds not overlain by loose covers of cinder, suggesting that these and other near-vent constructs can be accounted for by either the jet column fallout model or a ballistic model with drag. The two descriptions are found to be essentially mathematically equivalent and to represent two ways of thinking about the same process. The numerical experiments on ejecta construct growth failed to account for the aspect ratios of cinder cones but novel analogue experiments reproduced the ratios surprisingly well, allowing a simple explanation to be derived for them.

Acknowledgements

This work is dedicated to the courageous people of Heimaey who did not give up in 1973 when disaster struck. This work was developed while C.R. was visiting Bristol for 6 months, funded through the EU Training Network in Volcanology (Thank you!). C.R. wants to acknowledge the Christian-Albrechts-Universität Kiel for support, which granted him the space and time to develop this work during and after his stay in the UK. G.G.J.E. thanks the Nuffield Foundation (NAL Award) and the Fondation Belge de la Vocation for generous support (Golden Clover Prize). G.G.J.E. was an NSF-funded Visiting Scientist at Michigan Tech when this work was completed and thanks W.I. Rose and MTU colleagues for

their hospitality and support. G.G.J.E. thanks the Belgian Science Foundation (FWO Vlaanderen) and colleagues at Ghent University (Belgium) for current support. R.S.J. Sparks, G.P.L. Walker, O. Melnik, O. Matías and E. Suh made helpful suggestions that improved the manuscript. Last but not least we want to thank Prof. L. Wilson for editorial assistence and E. Parfitt and K. Bemis for constructive and helpful reviews.

References

Allen, J.R.L., 1985. Principles of Physical Sedimentology. Allen and Unwin, 272 pp.

Arrighi, S., Principe, C., Rosi, M., 2001. Violent strombolian and subplinian eruptions at Vesuvius during post-1631 activity. Bull. Volcanol. 63, 126–150.

Bagnold, R.A., 1941. The Physics of Blown Sand and Desert Dunes. Methuen, London, 265 pp.

Banks, N., Koyanagi, R., Honma, K., 1983. North Pagan (Mariana Islands). Bull. Volcan. Erup.

Barabasi, A.L., Albert, R., Schiffer, P., 1999. The physics of sand castles: maximum angle of stability in wet and dry granular media. Physics A 266, 366–371.

Behncke, B., 2001. The 2001 summit and flank eruption of Mt Etna. http://www.geo.mtu.edu/~boris/ETNA_2001.html.

Behncke, B., Neri, M., 2002. The July-August 2001 eruption of Mt Etna (Sicily). Bull. Volcanol., in review.

Bemis, K., 1995. A morphometric study of volcanoes in Guatemala, Iceland, the Snake River plains and the South Pacific. Ph.D. Thesis, Rutgers Univ., NJ, 254 pp.

Bemis, K., Bonar, D.E., 1997. Models of cinder cone growth, the effects of ballistic drag and grain flow. Geol. Soc. Am. Annual Meeting Abstract with Progr.

Blackburn, E.A., Wilson, L., Sparks, R.S.J., 1976. Mechanisms and dynamics of strombolian activity. J. Geol. Soc. Lond. 132, 429–440.

Bonadonna, C., Ernst, G.G.J., Sparks, R.S.J., 1998. Thickness variations and volume estimates of tephra fall deposits: The importance of particle Reynolds number. J. Volcanol. Geotherm. Res. 81, 173–189.

Bonis, S., Salazar, O., 1973. The 1971 and 1973 eruptions of Volcán Fuego, Guatemala, and some socio-economic considerations for the volcanologist. Bull. Volcanol. 37, 394–400.

Bowman, S.D., Watters, R.J., Zimbelman, D.R., Crowley, J.K., 1998. Methodology for rock mass strength assessment and results from edifice rocks, Mt. Rainier and Mt. Hood, USA. EOS Trans. AGU Fall Meeting 98, Abstract volume.

Brown, R.L., Richards, J.C., 1970. Principles of Powder Mechanics. Pergamon Press, Oxford.

Budnikov, V.A., Markhinin, Y.K., Ovsyannikov, A.A., 1983. The quantity, distribution and petrochemical features of pyroclastics of the Great Tolbachik eruption. In: Fedotov, S.A., Markhinin, Ye.K. (Eds.), The Great Tolbachik Fissure Eruption. Cambridge University Press, pp. 41–56.

Calvari, S., Pinkerton, H., 2002. Growth and incipient failure of the 'Laghetto' cinder cone during the 2001 Etna eruption, Geophys. Res. Abstr., 27th General Assembly of the EGS, Nice, Vol. 4.

Carn, S.A., 2000. The Lamonggan volcanic field, East Java, Indonesia: Physical volcanology, historic activity and hazards. J. Volcanol. Geotherm. Res. 95, 81–108.

Carracedo, J.C. et al., 1992. The 1730-1736 eruption of Lanzarote, Canary Islands - A long, high-magnitude basaltic fissure eruption. J. Volcanol. Geotherm. Res. 53, 239–250.

Cas, R.A.F., Wright, J.V., 1987. Volcanic Successions. Allen and Unwin, London, 528 pp.

Chouet, B.A., Hamisevicz, B., McGetchin, T.R., 1974. Photoballistics of volcanic jet activity at Stromboli, Italy. J. Geophys. Res. 79, 4961–4976.

Connor, C.B., Conway, F.M., 2000. Basaltic volcanic fields. In: Sigurdsson, H., Houghton, B., McNutt, S.R., Rymer, H., Stix, J. (Eds.), Encyclopedia of Volcanoes. Academic Press, New York, pp. 331–343.

Connor, C.B., Hill, B.E., Winfrey, B., Franklin, N.M., LaFemina, P.C., 2001. Estimation of volcanic hazards from tephra fallout. Nat. Hazards Rev. 2, 33–42.

Connor, C.B., Stamatakos, J., Ferrill, D., Hill, B.E., Ofoegbu, G., Conway, F.M., 2000. Volcanic hazards at the proposed Yucca Mountain, Nevada, high-level radioactive waste repository. J. Geophys. Res. 105, 417–432.

Cooke, R.S.J., 1975. Long Island and Ulawun (Papua New Guinea). Bull. Volcanic. Erup., 73–12.

Coulomb, C.A., 1773. Essai sur une application de règles de maximis et minimis a quelques problèmes de statique relatifs à l'architecture. Mém. Math. Phys. Acad. R. Sci. Paris 7, 343–382.

Dehn, J., 1987. Model of cinder cone formation. M.Sc. Thesis, Arizona State University, Tempe, AZ, 85 pp.

DiVito, M., Lirer, L., Mastrolorenzo, G., Rolandi, G., 1987. The 1538 Monte Nuevo eruption (Campi Flegrei, Italy). Bull. Volcanol. 49, 608–615.

Dohrenwend, J.C., Wells, S.G., Turrin, B.D., 1986. Degradation of Quartenary cinder cones in the Cima Volcanic Field, Mojave Desert, California. Geol. Soc. Am. Bull. 97, 421–427.

Earthquake Research Institute (ERI), 1988. The 1986-87 eruption of Izu-Oshima volcano. Heiwado Printing, Tokyo.

Ernst, G.G.J., 1996. Dynamics of sediment-laden plumes. Ph.D. Thesis, Dept. Earth Sciences, Univ. Bristol, U.K., 223 pp.

Ernst, G.G.J., Sparks, R.S.J., Carey, S.N., Bursik, M.I., 1996. Sedimentation from turbulent jets and plumes. J. Geophys. Res. 101, 5575–5589.

Fagents, S.A., Pace, K., Greeley, R., 2002. Origins of small volcanic cones on Mars. Lunar Planet. Sci. 33.

Ferreira, T., 2000. Caracterizao da actividade vulcanica recente da ilha de Sao Miguel: vulcanismo basaltico subaereo e zonas de desgaseificao. Avaliacao de riscos (in Portu-

guese). Ph.D. Thesis, Universidade dos Açores, Ponta Delgada, Portugal.
Fierstein, J., Hildreth, W., 1992. The plinian eruptions of 1912 at Novarupta, Katmai National Park, Alaska. Bull. Volcanol. 54, 646–684.
Fierstein, J., Houghton, B.F., Wilson, C.J.N., Hildreth, W., 1997. Complexities of plinian fall deposition at vent: an example from 1912 Novarupta eruption (Alaska). J. Volcanol. Geotherm. Res. 76, 215–227.
Foshag, W.F., Gonzalez, J., 1956. Birth and development of Parícutin volcano, Mexico. USGS Bull. 965-D, 355–489.
Global Volcanism Network, 1973. Vestmannaeyjar (Iceland). Bull. Glob. Volc. Network 1/71.
Global Volcanism Network, 1989. Lonquimay (Chile). Bull. Glob. Volc. Network 5/89.
Global Volcanism Network, 1995a. Cerro Negro (Nicaragua). Bull. Glob. Volc. Network 20, 12.
Global Volcanism Network, 1995b. Cerro Negro (Nicaragua), Bull. Glob. Volc. Network 20, 9.
Global Volcanism Network, 1995c. Fogo (Cape Verde Islands), Bull. Glob. Volc. Network 20, 3.
Green, J., Short, N.M., 1971. Volcanic Landforms and Surface Features: A Photographic Atlas and Glossary. Springer, 519 pp.
Guest, J.E., Bulmer, M.H., Aubele Beratan, J.K., Greeley, R., Head, J.W., Michaels, G., Weitz, C., Wiles, C., 1992. Small volcanic edifices and volcanism in the plains of Venus. J. Geophys. Res. 97, 15949–15966.
Handin, J., 1966. The Geological Society of America Memoir 97, Handbook of Physical Constants, Strength and Ductility. Geol. Soc. Am., 587 pp.
Hasenaka, T., Carmichael, I.S.E., 1985. The cinder cones of Michoacan-Guajanato, Central Mexico: Their age, volume and distribution, and magma discharge rate. J. Volcanol. Geotherm. Res. 25, 105–124.
Head, J.W., Wilson, L., 1989. Basaltic pyroclastic eruptions: influence of gas-release patterns and volume fluxes on fountain structure, and the formation of cinder cones, spatter cones, rootless flows, lava ponds and lava flows. J. Volcanol. Geotherm. Res. 37, 261–271.
Heiken, G., 1978. Characteristics of tephra from Cinder Cone, Lassen Volcanic National Park, California. Bull. Vulcanol. 41, 119–130.
Heiken, G., 2003. Industrial use of volcanic materials. In: Martí, J., Ernst, G.G.J. (Eds.), Volcanoes and the Environment. Cambridge University Press, in press.
Hildreth, W., Drake, R.E., 1992. Volcán Quizapú, Chilean Andes. Bull. Vulcanol. 54, 93–125.
Hill, B.E., Connor, C.B., Jarzemba, M.S., LaFemina, P.C., Navarro, M., Strauch, W., 1998. 1995 eruptions of Cerro Negro volcano, Nicaragua, and risk assessment for future eruptions. Geol. Soc. Am. Bull. 1110, 1231–1241.
Houghton, B.F., Schmincke, H.U., 1989. Rothenberg scoria cone, East Eifel: A complex strombolian and phreatomagmatic volcano. Bull. Volcanol. 52, 28–48.
Houghton, B.F., Wilson, C.J.N., Smith, I.E.M., 1999. Shallow-seated controls on styles of explosive basaltic volcanism: a case study from New Zealand. J. Volcanol. Geotherm. Res. 99, 97–120.
Jaupart, C., Vergniolle, S., 1997. Laboratory models of Hawaiian and Strombolian eruptions. Nature 331, 518–520.
Kammel, D.A., 1997. Physical characteristics of alternative feeds (as stored, handled and fed). In: Nutrition and Feeding. National Dairy Database, Univ. Maryland.
Kestelman, H., 1960. Modern Theories of Integration, 2nd edn. Dover, New York.
Knudsen, J.G., Katz, D.L., 1958. Fluid Dynamics and Heat Transfer. McGraw-Hill, New York.
Krafft, M., Gerente, A., 1977. L'activité du Piton de la Fournaise entre Oct. 1972 et Mai 1973. C.R. Acad. Sci. Paris D 24, 607–610.
Luhr, J.F., Simkin, T., 1993. Parícutin: The Volcano Born in a Mexican Cornfield. Geoscience Press, Phoenix, AZ, 427 pp.
Macdonald, G.A., 1972. Volcanoes. Prentice-Hall, Englewood Cliffs, 510 pp.
McClelland, L., Simkin, T., Sumners, M., Nielsen, E., Stein, T.C., 1989. Global volcanism 1975-1985. Smithsonian Institution Scientific Event Alert Network (SEAN), Prentice Hall, NJ.
McGetchin, T.R., Head, J.W., 1973. Lunar cinder cones. Science 180, 68–71.
McGetchin, T.R., Settle, M., Chouet, B.A., 1974. Cinder cone growth modelled after North East crater, Mt Etna, Sicily. J. Geophys. Res. 79, 3257–3272.
McInnes, B.I.A., Gregoire, M., Binns, R.A., Herzig, P.M., Hannington, M.D., 2001. Hydrous metasomatism of oceanic sub-arc mantle, Lihir, Papua New Guinea: petrology and geochemistry of fluid-metasomatised mantle wedge xenoliths. Earth Planet. Sci. Lett. 188, 169–183.
McKnight, S.B., Williams, S.N., 1997. Old cinder cone or young composite volcano? The nature of Cerro Negro, Nicaragua. Geology 25, 339–342.
Magus'kin, M.A., Enman, V.B., Tselichev, V.S., 1983. Changes in height, volume and shape of the New Tolbachik volcanoes of the Northern Breakthrough. In: Fedotov, S.A., Markhinin, Ye.K. (Eds.), The Great Tolbachik Fissure Eruption. Cambridge University Press, pp. 307–315.
Martí, J., Ablay, G.J., Redshaw, L.T., Sparks, R.S.J., 1994. Experimental studies of collapse calderas. J. Geol. Soc. Lond. 151, 919–929.
Matthews, R.A., Franks, A.L., 1971. Cinder cone sewage disposal site at north Lake Tahoe. Calif. Geol. 24, 183–195.
Melnik, O.E., 1996. Unsteady phenomena in the volcanic eruption dynamics of high-viscosity gas saturated magmas, translated from Izvestiya Rossiiskoi Akademii Nauk on http://gfd.gly.bris.ac.uk/gfd-people/oleg.melnik/volino.htm.
Miller, R.L., Byrne, R.J., 1966. The angle of repose for a single grain on a fixed rough bed. Sedimentology 6, 303–314.
Montaggioni, L., Nativel, P., Billard, G., 1972. L'activité actuelle du Piton de la Fournaise. C.R. Acad. Sci. Paris D 275, 2615–2618.
Neal, C.A., Wolfe, E.W., Greenland, L.P., 1987. Pu'u'O'o II: A summary of episodes 4-20. In: Decker, R.W., Halbig,

J.B., Hazlett, R.W., Okamura, R., Wright, T.L. (Eds.), Hawaii Symposium on How Volcanoes Work, Hilo, HI, Jan. 19–25, 1987, Abstract vol. p. 189.
Oda, M., Iwashita, K., 1997. Mechanisms of Granular Material - An Introduction. Balkema, Rotterdam.
Parfitt, E.A., 1998. A study of clast size distributions, ash deposition and fragmentation in Hawaiian-style volcanic eruptions. J. Volcanol. Geotherm. Res. 84, 197–208.
Parfitt, E.A., Wilson, L., 1995. Explosive volcanic eruptions - IX. The transition between Hawaiian-style lava fountaining and Strombolian explosive activity. Geophys. J. Int. 121, 226–232.
Parfitt, E.A., Wilson, L., 1999. A Plinian treatment of fallout from Hawaiian lava fountains. J. Volcanol. Geotherm. Res. 88, 67–75.
Pfeiffer, T., 2001. http://www.geo.aau.dk/palstrat/tom/santorini_homepage/volcanoes/etna0701_2.htm.
Porter, S.C., 1972. Distribution, morphology and size frequency of cinder cones on Mauna Kea volcano, Hawaii. Geol. Soc. Am. Bull. 83, 3607–3612.
Richter, D.H., Eaton, J.P., Murata, K.J., Ault, W.U., Krivoy, H.L., 1970. Chronological narrative of the 1959-60 eruption of Kilauea volcano, Hawaii. U.S. Geol. Surv. Prof. Paper 537-E, 73 pp.
Rittmann, A., 1938. Die Vulkane am Myvatn in Nordost-Island. Bull. Volcanol. 4, 3–38.
Roche, O., Druitt, T., Merle, O., 2000. Experimental study of caldera formation. J. Geophys. Res. 105, 395–416.
Rose, W.I., Anderson, A.T., Woodruff, L.G., Bonis, S.B., 1978. The October 1974 basaltic tephra from Fuego Volcano: Description and history of the magma body. J. Volcanol. Geotherm. Res. 4, 3–53.
Scientific Event Alert Network (SEAN), 1974. La Palma (Canary Islands). Volcanic activity reports 10-11/71.
Scientific Event Alert Network (SEAN), 1986. Pacaya, Guatemala, 11/12.
Scientific Event Alert Network (SEAN), 1988. Lonquimay (Chile), SEAN 5/89.
Self, S., 1976. The recent volcanology of Terceira. J. Geol. Soc. Lond. 132, 645–666.
Self, S., Sparks, R.S.J., Booth, B., Walker, G.P.L., 1974. The 1973 Heimaey strombolian scoria deposit, Iceland. Geol. Mag. 111, 539–548.
Settle, M., 1979. The structure and emplacement of cinder cone fields. Am. J. Sci. 279, 1089–1107.
Sheridan, M.F., 1971. Particle-size characteristics of pyroclastic tuffs. J. Geophys. Res. 23, 5627–5634.
Sheridan, M., Wohletz, K.H., 1983. Hydrovolcanism: Basic considerations and review. J. Volcanol. Geotherm. Res. 17, 1–29.
Siebe, C., 2000. Age and archaeological implications of Xitle volcano, southwestern basin of Mexico City. J. Volcanol. Geotherm. Res. 104, 45–64.
Simkin, T., Siebert, L., 1994. Volcanoes of the World: Catalogue of Active Volcanoes, 2nd edn. Geoscience Press, Tucson, AZ.
Sohn, Y.K., 1996. Hydrovolcanic processes forming basaltic tuff rings and cones on Cheju Island, Korea. Geol. Soc. Am. Bull. 108, 119–1211.
Sohn, Y.K., Park, K.H., 2003. Geomorphology of hydromagmatic volcanoes in Jeju Island, Korea. Earth Planet. Sci. Lett., in review.
Sparks, R.S.J., Bursik, M.I., Carey, S.N., Gilbert, J.S., Glaze, L.S., Sigurdsson, H., Woods, A.W., 1997. Volcanic Plumes. Wiley, New York, 574 pp.
Spudis, P.D., 2000. Volcanism on the Moon. In: Sigurdsson, H., Houghton, B., McNutt, S.R., Rymer, H., Stix, J. (Eds.), Encyclopedia of Volcanoes. Academic Press, New York, pp. 697–708.
Sumner, J.M., 1998. Formation of clastogenic lava flows during fissure eruption and scoria cone collapse: the 1986 eruption of Izu-Oshima Volcano, eastern Japan. Bull. Volcanol. 60, 195–212.
Suradjat, J.A., Siswowidjo, S., 1984. Galunggung (Indonesia). Bull. Volcan. Erup.
Thompson, R.B., 1973. Tinakula (Solomon Islands). Bull. Volcan. Erup.
Thorarinsson, S., 1964. Surtsey: The New Island in the North Atlantic. Viking Press, New York.
Thorarinsson, S., Steinthorsson, S., Einarsson, Th., Kristmannsdottir, H., Oskarsson, N., 1973. The eruption on Heimaey, Iceland. Nature 241, 372–375.
Tokarev, P.I., 1983. Calculation of the magma discharge, growth in the height of the cone and dimensions of the feeder channel of crater 1 in the Great Tolbachik fissure eruption, July 1975. In: Fedotov, S.A., Markhinin, Ye.K. (Eds.), The Great Tolbachik Fissure Eruption. Cambridge University Press, pp. 27–35.
Tomasson, J., 1967. On the origin of sedimentary water beneath the Vestman Islands. Jökull 17, 300–311.
Tüzün, U., 1979. Velocity distribution in funnel-flow bins. Ph.D. Thesis, University of Cambridge, Churchill College.
Tüzün, U., Nedderman, R.M., 1982. An investigation of the flow boundary during steady-state discharge from a funnel-flow bunker. Powder Technol. 31, 27–43.
Van Burkalow, A., 1945. Angle of repose and angle of sliding friction: an experimental study. Geol. Soc. Am. Bull. 56, 669–708.
Vergniolle, S., Brandeis, G., Mareschal, J.-C., 1996. Strombolian explosions: Eruption dynamics determined from acoustic measurements. J. Geophys. Res. 101, 20449–20466.
Vergniolle, S., Mangan, M., 2000. Hawaiian and Strombolian eruptions. In: Sigurdsson, H., Houghton, B., McNutt, S.R., Rymer, H., Stix, J. (Eds.), Encyclopedia of Volcanoes. Academic Press, New York, pp. 447–461.
Verwoerd, W.J., Russell, S., Berruti, A., 1981. 1980 Volcanic eruption reported on Marion Island. Earth Planet. Sci. Lett. 54, 153–156.
Vespermann, D., Schmincke, H.-U., 2000. Scoria cones and tuff rings. In: Sigurdsson, H., Houghton, B., McNutt, S.R., Rymer, H., Stix, J., Eds., Encyclopedia of Volcanoes. Academic Press, New York, pp. 683–694.
Walker, G.P.L., 1973. Explosive volcanic eruptions- a new classification scheme. Geol. Rundsch. 62, 431–446.

Walker, G.P.L., Self, S., Wilson, L., 1984. Tarawera 1886 New Zealand - A basaltic plinian fissure eruptions. J. Volcanol. Geotherm. Res. 21, 61–78.

Walter, T.R., Troll, V.R., 2001. Formation of caldera periphery faults: an experimental study. Bull. Volcanol. 63, 191–203.

Wilson, L., Head, J.W., 1994. Mars: Review and analysis of volcanic eruption theory and relationships to observed landforms. Rev. Geophys. 32, 248–268.

Wohletz, K.H., 1986. Explosive magma-water interactions: Thermodynamics, explosion mechanisms and field studies. Bull. Volcanol. 48, 245–264.

Wohletz, K.H., Sheridan, M.F., 1983. Hydrovolcanic explosions. II. Evolution of basaltic tuff rings and tuff cones. Am. J. Sci. 183, 385–413.

Wolfe, E.W., Neal, C.A., Banks, N.G., Dunggan, T.J., 1988. Geologic observations and chronology of eruptive vents. In: Wolfe, E.W. (Ed.), The Pu'u'O'o eruption of Kilauea volcano, Hawaii, Episodes 1-20, Jan. 3, through June 8, 1984. USGS Prof. Pap. 1463, 1–97.

Wood, C.A., 1977. Cinder cones on Earth, Moon and Mars. EOS Trans. AGU 58, 425.

Wood, C.A., 1980. Morphometric evolution of cinder cones. J. Volcanol. Geotherm. Res. 7, 387–413.

Yasui, M., Koyaguchi, T., 1998. Formation of a pyroclastic cone in the 1783 plinian eruptions of Asama volcano. Bull. Volcanol. Soc. Jpn. 43, 457–465.

Yasui, M., Koyaguchi, T., Aramaki, S., 1997. Plinian eruptions in the 1783 activity of Asama volcano inferred from the deposits and the old records. Bull. Volcanol. Soc. Jpn. 42, 281–297.

Yucca Mountain Project Website, 2002. http://www.ymp.gov/.